

ARTICLE

Hlf marks the developmental pathway for hematopoietic stem cells but not for erythro-myeloid progenitors

Tomomasa Yokomizo^{1,2,3}, Naoki Watanabe², Terumasa Umemoto¹, Junichi Matsuo³, Ryota Harai¹, Yoshihiko Kihara^{2,4}, Eri Nakamura⁵, Norihiro Tada⁵, Tomohiko Sato⁶, Tomoiku Takaku², Akihiko Shimono³, Hitoshi Takizawa¹, Naomi Nakagata⁷, Seiichi Mori⁸, Mineo Kurokawa⁶, Daniel G. Tenen^{3,9}, Motomi Osato^{1,3}, Toshio Suda^{1,3}, and Norio Komatsu²

Before the emergence of hematopoietic stem cells (HSCs), lineage-restricted progenitors, such as erythro-myeloid progenitors (EMPs), are detected in the embryo or in pluripotent stem cell cultures in vitro. Although both HSCs and EMPs are derived from hemogenic endothelium, it remains unclear how and when these two developmental programs are segregated during ontogeny. Here, we show that hepatic leukemia factor (Hlf) expression specifically marks a developmental continuum between HSC precursors and HSCs. Using the *Hlf*-tdTomato reporter mouse, we found that *Hlf* is expressed in intra-aortic hematopoietic clusters and fetal liver HSCs. In contrast, EMPs and yolk sac hematopoietic clusters before embryonic day 9.5 do not express *Hlf*. HSC specification, regulated by the *Evi-1/Hlf* axis, is activated only within *Hlf*⁺ nascent hematopoietic clusters. These results strongly suggest that HSCs and EMPs are generated from distinct cohorts of hemogenic endothelium. Selective induction of the *Hlf*⁺ lineage pathway may lead to the in vitro generation of HSCs from pluripotent stem cells.

Introduction

Hematopoietic stem cells (HSCs), which reside in the bone marrow, are the major source of mature blood lineages including myeloid cells and lymphocytes (Orkin and Zon, 2008). In the mouse embryo during midgestation, HSCs are generated from aortic endothelium through the transdifferentiation process known as endothelial-to-hematopoietic transition (EHT; Zovein et al., 2008; Chen et al., 2009; Medvinsky et al., 2011). During EHT, flat-shaped hemogenic endothelia transform into round-shaped hematopoietic cells (Boisset et al., 2010), which subsequently form cell aggregates, called hematopoietic clusters (Yokomizo and Dzierzak, 2010). At embryonic days (E) 10–11, these clusters are thought to contain HSC precursors (pre-HSCs; Taoudi et al., 2008; Zhou et al., 2016), which colonize the fetal liver before or after they mature into fully functional HSCs. It has been reported that HSCs are generated from regions other than the dorsal aorta, such as the yolk sac, placenta, and head (Samokhvalov et al., 2007; Rhodes et al., 2008; Li et al., 2012). Indeed, a recent tracing study revealed that 35%–40% of HSCs in

the adult bone marrow may originate from the yolk sac (Lee et al., 2016).

Before the emergence of HSCs (~E10), lineage-restricted progenitors, such as erythro-myeloid progenitors (EMPs) and lymphoid-myeloid progenitors, are detected in the mouse embryo (Böiers et al., 2013; McGrath et al., 2015a). These are referred to as HSC-independent lineages (Dzierzak and Bigas, 2018). EMPs are the dominant progenitor population at the midgestation stage and produce transient, definitive-type erythrocytes and long-lived, tissue-resident macrophages, which have the potential to proliferate and are maintained in some tissues until adult stage and thereafter (Perdiguerro et al., 2015). Similar to aortic clusters, EMPs are generated from hemogenic endothelium at E8–9 in the yolk sac through the formation of hematopoietic clusters (Padrón-Barthe et al., 2014; Frame et al., 2016; Kasaai et al., 2017).

Based on the results of a transgenic rescue experiment that used the unique features of *Ly6a* and *Tek* regulatory elements, it

¹International Research Center for Medical Sciences, Kumamoto University, Kumamoto, Japan; ²Department of Hematology, Juntendo University Graduate School of Medicine, Tokyo, Japan; ³Cancer Science Institute of Singapore, National University of Singapore, Singapore; ⁴Leading Center for the Development and Research of Cancer Medicine, Juntendo University Graduate School of Medicine, Tokyo, Japan; ⁵Laboratory of Genome Research, Research Institute for Diseases of Old Age, Juntendo University Graduate School of Medicine, Tokyo, Japan; ⁶Department of Hematology and Oncology, Graduate School of Medicine, The University of Tokyo, Tokyo, Japan; ⁷Division of Reproductive Engineering, Center for Animal Resources and Development, Kumamoto University, Kumamoto, Japan; ⁸Division of Cancer Genomics, Cancer Institute of Japanese Foundation for Cancer Research, Tokyo, Japan; ⁹Harvard Stem Cell Institute, Boston, MA.

Correspondence to Tomomasa Yokomizo: tomoyokomizo@gmail.com; Toshio Suda: csits@nus.edu.sg.

© 2019 Yokomizo et al. This article is distributed under the terms of an Attribution–Noncommercial–Share Alike–No Mirror Sites license for the first six months after the publication date (see <http://www.rupress.org/terms/>). After six months it is available under a Creative Commons License (Attribution–Noncommercial–Share Alike 4.0 International license, as described at <https://creativecommons.org/licenses/by-nc-sa/4.0/>).

has been proposed that HSCs and EMPs arise from distinct hemogenic endothelium (Chen et al., 2011). However, it is still difficult to identify HSC-producing endothelium due to the lack of specific markers, an issue that also hinders the generation of HSCs from pluripotent stem cells in vitro (Rowe et al., 2016). So far, HSC induction without the introduction of genetic materials has not been achieved, whereas EMPs are readily induced, suggesting that current standard culture conditions do not recapitulate the HSC-generating phase of hematopoiesis in the aorta-gonad-mesonephros (AGM) region but rather mimic the EMP-forming situation in the yolk sac (McGrath et al., 2015a). One way to circumvent this issue is the identification of nascent pre-HSC/HSC specific markers suitable for optimizing culture conditions (Li et al., 2017; Tober et al., 2018).

Hepatic leukemia factor (Hlf) encodes a proline- and acid-rich basic region leucine zipper (PAR-bZIP) transcription factor, and recent studies revealed that Hlf is specifically expressed in adult bone marrow HSCs and is a critical regulator of HSC quiescence (Komorowska et al., 2017; Wahlestedt et al., 2017). Patients with acute lymphoblastic leukemia have a reciprocal chromosomal translocation of *Hlf* with *E2A* gene (Inaba et al., 1992). In addition, several studies have shown through forced expression that Hlf expression is strongly associated with the acquisition of stem cell properties. Indeed, the ectopic expression of Hlf in HSCs/progenitors reinforces multipotency and self-renewal ability (Shojaei et al., 2005; Gazit et al., 2013). Six transcription factors, including Hlf, can reprogram blood progenitors into transplantable HSC-like cells (Riddell et al., 2014).

Here, using a novel reporter mouse, we analyzed *Hlf* expression during hematopoietic development in the embryo. *Hlf* expression begins in E10 aortic clusters during EHT, and Hlf^{hi} cell fractions in E14 fetal livers are enriched for HSCs that can reconstitute the adult hematopoietic system. In contrast, *Hlf* expression is not detected in EMPs or in hematopoietic clusters in E9 yolk sac. These results suggest that *Hlf* expression discriminates the HSC-producing pathway from the EMP-producing pathway in the mouse embryo.

Results

Generation of *Hlf*^{tdTomato} knock-in mouse

To understand HSC specification during ontogeny and to search for nascent HSC markers, we performed single-cell microarray analysis of developing HSC populations. We previously showed that hematopoietic clusters in the major arteries can be detected and enriched by c-Kit and CD31 staining and that *Runx1-GFP* (*eRI-GFP*) transgene expression marks hemogenic endothelial cells (Ng et al., 2010; Yokomizo and Dzierzak, 2010). Using these markers, we collected 85 single cells from five different populations: endothelial cells (*eRI-GFP*-CD31⁺Ter119⁻CD45⁻CD41⁻), hemogenic endothelial cells (*eRI-GFP*-CD31⁺Ter119⁻CD45⁻CD41⁻), E10.5 hematopoietic clusters (*c-Kit*⁺CD31⁺CD45⁺SSEA1⁻), E12.5 hematopoietic clusters (*c-Kit*⁺CD31⁺CD45⁺SSEA1⁻), and E14.5 fetal liver HSCs (CD150⁺CD48⁻c-Kit⁺Sca-1⁺Lin⁻Mac-1⁻; Fig. S1). Subsequent cDNA synthesis and microarray analysis revealed a dynamic change in hematopoietic gene expression during HSC development (Fig. 1 A). Among HSC/hematopoietic stem and

progenitor cell (HSPC)-related genes, four genes—*Mecom*, *Hlf*, *Hoxa9*, and *Procr*—showed differential expression patterns compared with other genes (such as *Gata2*, *Myb*, and *Meis1*) and seemed to be up-regulated during HSC development (Fig. 1 A). Because endothelial cells could be an obstacle for imaging or identifying rare cell populations, such as HSCs and pre-HSCs, we excluded *Mecom*, *Hoxa9*, and *Procr* from the list of candidate marker genes, as they are expressed in sorted hemogenic endothelial fractions (Fig. 1 A). Therefore, we focused on *Hlf* for further detailed analysis.

Hlf encodes the PAR-bZIP transcription factor and is expressed in adult HSCs (Gazit et al., 2013; Komorowska et al., 2017). To further investigate *Hlf* expression during HSC formation in the embryo, we generated an *Hlf* reporter mouse. For the *Hlf*-tdTomato allele, we inserted the sequence encoding T2A-tdTomato before the endogenous stop codon within exon 4 (Fig. 1 B). This should leave endogenous *Hlf* expression intact in the mice. Indeed, a similar level of Hlf protein expression was observed between *Hlf*^{f/+} and *Hlf*^{tdTomato/+} mice (Fig. S2 A). Blood cell analysis also showed normal hematopoietic differentiation in adult *Hlf*^{tdTomato/+} mice (Fig. S2, B and C).

Hlf is predominantly expressed in fetal liver HSCs

To investigate *Hlf* expression in embryonic hematopoiesis, we first analyzed the *Hlf*^{tdTomato/+} fetal liver at E14.5. In flow cytometry analysis, 3.9% ± 1.0% of fetal liver cells were positive for *Hlf*-tdTomato (Hlf⁺). Virtually all Hlf^{hi} cells were positive for c-Kit, and lineage marker-positive cells (Lin⁺) were negative for *Hlf* (Fig. 1, C and E), indicating that the expression is restricted to HSCs/progenitor cells. Immunostaining analysis of E14.5 fetal liver also showed restricted *Hlf* expression within a subset of c-Kit⁺ cells (Fig. 1 D). Within the c-Kit⁺ fraction, CD150⁺CD48⁻c-Kit⁺Sca-1⁺Lin⁻ (CD150⁺CD48⁻KSL) HSCs had the highest expression of *Hlf*, and the intensity decreased along with differentiation (Fig. 1 C). A similar expression pattern was also observed in the adult bone marrow (Fig. S2, D and E).

To confirm the correlation between *Hlf* expression and stem cell potential, we isolated cells with the highest (0.03%) and low/negative *Hlf* expression level (Hlf^{hi}c-Kit⁺ cells and Hlf^{lo/-}c-Kit⁺ cells, respectively) and transplanted them separately into irradiated adult mice (Fig. 1 E). Long-term repopulating activity was found for the Hlf^{hi} fraction but not the Hlf^{lo/-} fraction (Fig. 1 E). These data indicate that Hlf^{hi} cells include HSCs in the E14.5 fetal liver.

Hlf is specifically expressed in hematopoietic clusters in the dorsal aorta

Embryonic HSCs are generated from hemogenic endothelium through the formation of hematopoietic clusters within the dorsal aorta (Chen et al., 2009). To examine the expression of *Hlf* in the AGM region, we performed whole-mount immunostaining analysis of E10.5 *Hlf*^{tdTomato/+} embryos. *Hlf*-tdTomato signals were detected exclusively within the dorsal aorta (Fig. 2 A). Most (98%) of the c-Kit⁺ cells attached to the endothelial wall were positive for *Hlf* (Fig. 2, B-D). c-Kit⁺ hematopoietic clusters in the vitelline artery and the umbilical artery were also positive for *Hlf* (Fig. 2 E). On the other hand, endothelial cells

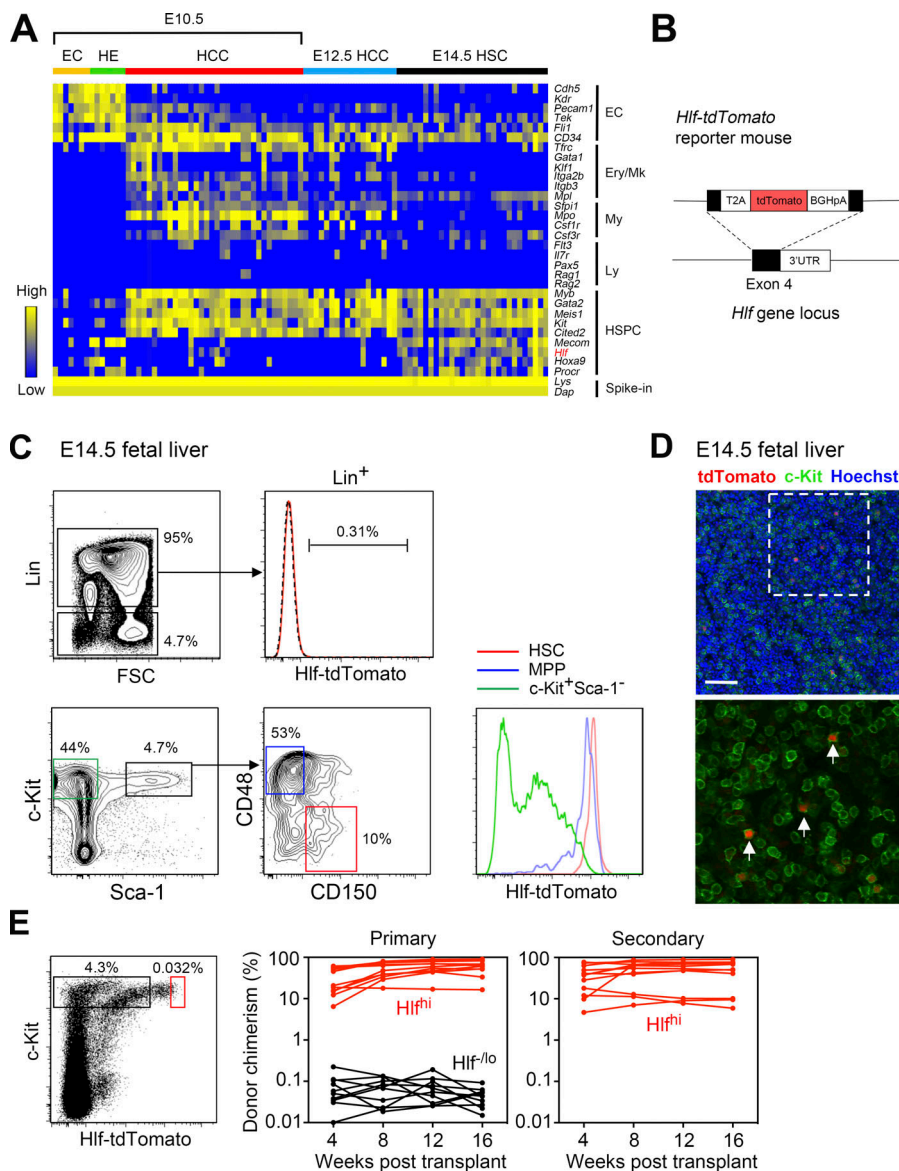


Figure 1. *Hlf* is predominantly expressed in fetal liver HSCs. (A) Heatmap showing differentially expressed genes in single-cell microarray data of developing HSC fractions: E10.5 endothelial cells (EC; seven cells), E10.5 hemogenic endothelial cells (HE; seven cells), E10.5 hematopoietic cluster cells (E10.5 HCC; 28 cells), E12.5 hematopoietic cluster cells (E12.5 HCC; 16 cells), and E14.5 HSC (27 cells). Flow cytometry gating used to isolate the population is shown in Fig. S1. Genes are categorized by known markers of hematopoietic and endothelial lineages. Microarray data are generated from 13 independent sorts. Ery/Mk, erythroid-megakaryocytic lineage; My, myeloid lineage; Ly, lymphoid lineage. (B) Targeting strategy of *Hlf*^{tdTomato} reporter mouse. (C) *Hlf*-tdTomato expression in E14.5 *Hlf*^{tdTomato/+} fetal liver. Flow cytometry analysis of hematopoietic lineages. Top right: *Hlf*-tdTomato expression in lineage-positive fraction from *Hlf*^{tdTomato/+} (red) and *Hlf*^{+/+} (black dashed) embryos. Data are representative of two independent experiments. MPP, multipotential progenitors. (D) Confocal image of *Hlf*-tdTomato expression in the fetal liver at E14.5. Arrows indicate tdTomato^{hi} cells. Scale bar, 50 μ m. (E) Transplantation experiments. Left: Flow cytometry sorting of *Hlf*^{hi} and *Hlf*^{lo/-} cells from E14.5 *Hlf*^{tdTomato/+} fetal liver. Irradiated mice were transplanted with 100 *Hlf*^{hi}-c-Kit⁺ cells or 5,000 *Hlf*^{lo/-}-c-Kit⁺ cells. Right: Total donor reconstitution over the time course of transplantation ($n = 10-12$). Combined data are from two experiments.

(CD31⁺c-Kit⁻) did not express *Hlf* (Fig. 2, B and C), indicating that *Hlf* starts to be expressed in nascent hematopoietic cells. Of note, 95% of the c-Kit⁺ circulating cells were negative for *Hlf* (Fig. 2 D), which, as shown later, may indicate a specific marking of the HSC-producing pathway in the dorsal aorta.

We also examined the expression of *Hlf*-tdTomato in the E10.5 caudal half region by FACS analysis. As expected, a distinct *Hlf*⁺c-Kit⁺ subset (0.051% \pm 0.014%) was detected, and endothelial cells (CD31⁺CD45⁻CD41⁻) were negative for *Hlf* (Fig. 2 F). The *Hlf*⁺c-Kit⁺ subset coexpressed CD41 and exhibited a heterogeneous expression of CD45, consistent with known characteristics of hematopoietic clusters (Yokomizo and Dzierzak, 2010). Because c-Kit⁺ circulating cells were not included in the *Hlf*⁺c-Kit⁺ subset (Fig. 2 D), this subset represents nearly a pure population of hematopoietic clusters.

Developing HSCs express high levels of *Hlf*

We noticed that the intensity of tdTomato in the E10 hematopoietic cluster cells was apparently weak compared with that in

the E14.5 HSCs. Given that HSC maturation occurs between E10.5 and E14.5 stages, we speculated that *Hlf* expression may be an indicator of HSC maturation. To explore this possibility, we compared *Hlf*-tdTomato expression between pre-HSCs and HSCs. A recent study showed that pre-HSCs are immunophenotypically defined by CD31⁺CD45⁻CD41^{lo}c-Kit⁺EPCR^{hi} cells (Zhou et al., 2016; Fig. S3 A). As expected, pre-HSCs reside in the hematopoietic cluster subset and, similar to HSCs in the E14.5 fetal liver, exhibited the highest intensity of *Hlf* expression in the AGM region (Fig. 3 A). *Hlf* expression in the pre-HSCs was lower than that in the E14.5 HSCs (Fig. 3 A). An increase in *Hlf* expression in the HSCs was observed until the adult stage (Fig. S3 B). These data suggest that *Hlf* expression increases with HSC development.

Hematopoietic clusters detached from aortic endothelium colonize the fetal liver via the circulation (Zovein et al., 2008). Therefore, it is plausible that pre-HSC to HSC maturation occurs in the dorsal aorta or fetal liver. To determine which organ provides the HSC maturation niche, we analyzed the expression

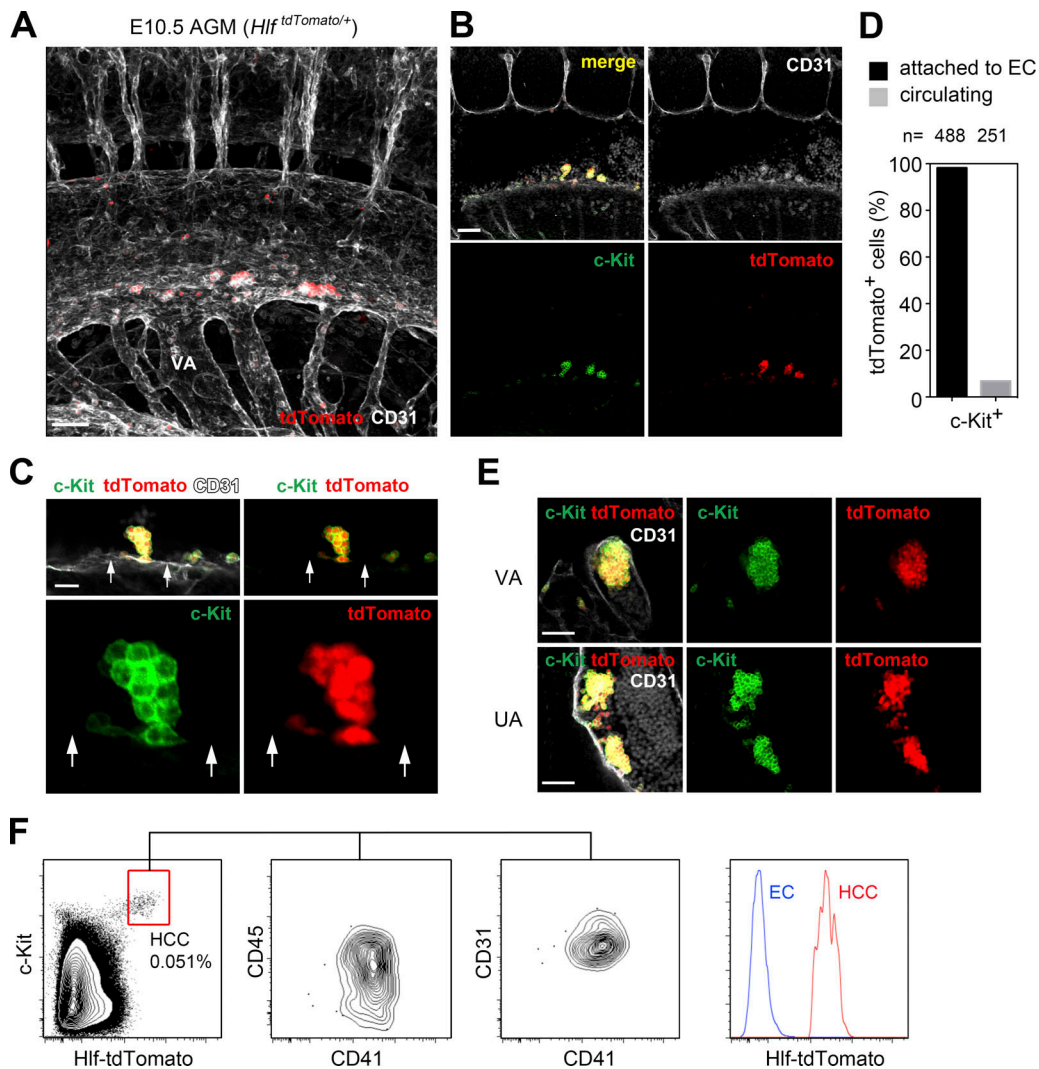


Figure 2. *Hlf* expression specifically marks hematopoietic clusters in the AGM region. (A–C) Whole-mount immunostaining of E10.5 *Hlf*^{tdTomato/+} mouse. **(A)** 3D confocal image of tdTomato (red) and CD31 (white) expression in the dorsal aorta at 34 sp. VA, vitelline artery. Scale bar, 50 μ m. **(B)** Sagittal image of dorsal aorta for tdTomato (red), c-Kit (green), and CD31 (white) expression at 36 sp. Scale bar, 50 μ m. **(C)** High-magnification view of a hematopoietic cluster in the dorsal aorta at 35 sp. Note that tdTomato expression is not observed in the endothelial cell layer (arrows). Scale bar, 25 μ m. **(D)** Frequency of tdTomato⁺ cells in the attached and circulating c-Kit⁺ cells (35 and 36 sp). Combined data are from three experiments. EC, endothelial cells. **(E)** Hematopoietic clusters in E10.5 (36 sp) vitelline and E10.5 (36 sp) umbilical arteries. VA, vitelline artery; UA, umbilical artery. Scale bars, 50 μ m. **(F)** Flow cytometry analysis of E10.5 *Hlf*^{tdTomato/+} caudal half region. HCC, hematopoietic cluster cells (*Hlf*⁺c-Kit⁺); EC, endothelial cells (CD31⁺CD45⁻CD41⁻). Data are representative of three independent experiments.

of *Hlf*-tdTomato within the AGM and fetal liver. As shown in Fig. 3 B, sequential up-regulation in *Hlf* was observed in the fetal liver, but not in the AGM after E12.5. Immunostaining analysis also showed an up-regulation in *Hlf*-tdTomato in the fetal liver between E11.5 and E14.5 (Fig. 3 C). A portion of the *Hlf*^{hi} cells in the fetal liver expressed Evi-1 and endothelial protein C receptor (EPCR), two markers of fetal liver HSCs (Iwasaki et al., 2010; Kataoka et al., 2011) that were both identified as embryonic HSC signature genes in our microarray analysis (Fig. 1 A). Both *Hlf*^{hi}Evi-1⁺ and *Hlf*^{hi}EPCR⁺ subsets were gradually apparent along with the elevation in *Hlf* expression between E11.5 and E14.5 (Fig. 3 D), supporting the notion that HSC maturation occurs within the *Hlf*^{hi} subset in the fetal liver. Localization of the developing HSCs within the *Hlf*^{hi} subset was confirmed by

long-term repopulation assay. *Hlf*^{hi} cells isolated from the E12.5 fetal liver gave long-term multilineage reconstitution (Fig. 3 E). Taken together, we conclude that *Hlf* expression marks developing HSCs in the embryo.

Hlf is not expressed in EMPs and their progenies

Before the formation of HSCs, EMPs emerge in the yolk sac and migrate to other organs via the circulation (Lux et al., 2008). Most c-Kit⁺ circulating cells at E10.5 are EMPs (Frame et al., 2016). Immunostaining analysis of the *Myb*^{GFP/+} knock-in reporter mouse, which presumably marks both HSCs and EMPs (Hoeffel and Ginhoux, 2015; Sakamoto et al., 2015), showed that c-Kit⁺ circulating cells in the dorsal aorta are positive for *Myb*-GFP (Fig. S4 A). On the other hand, analysis of *Hlf*^{tdTomato/+} mice

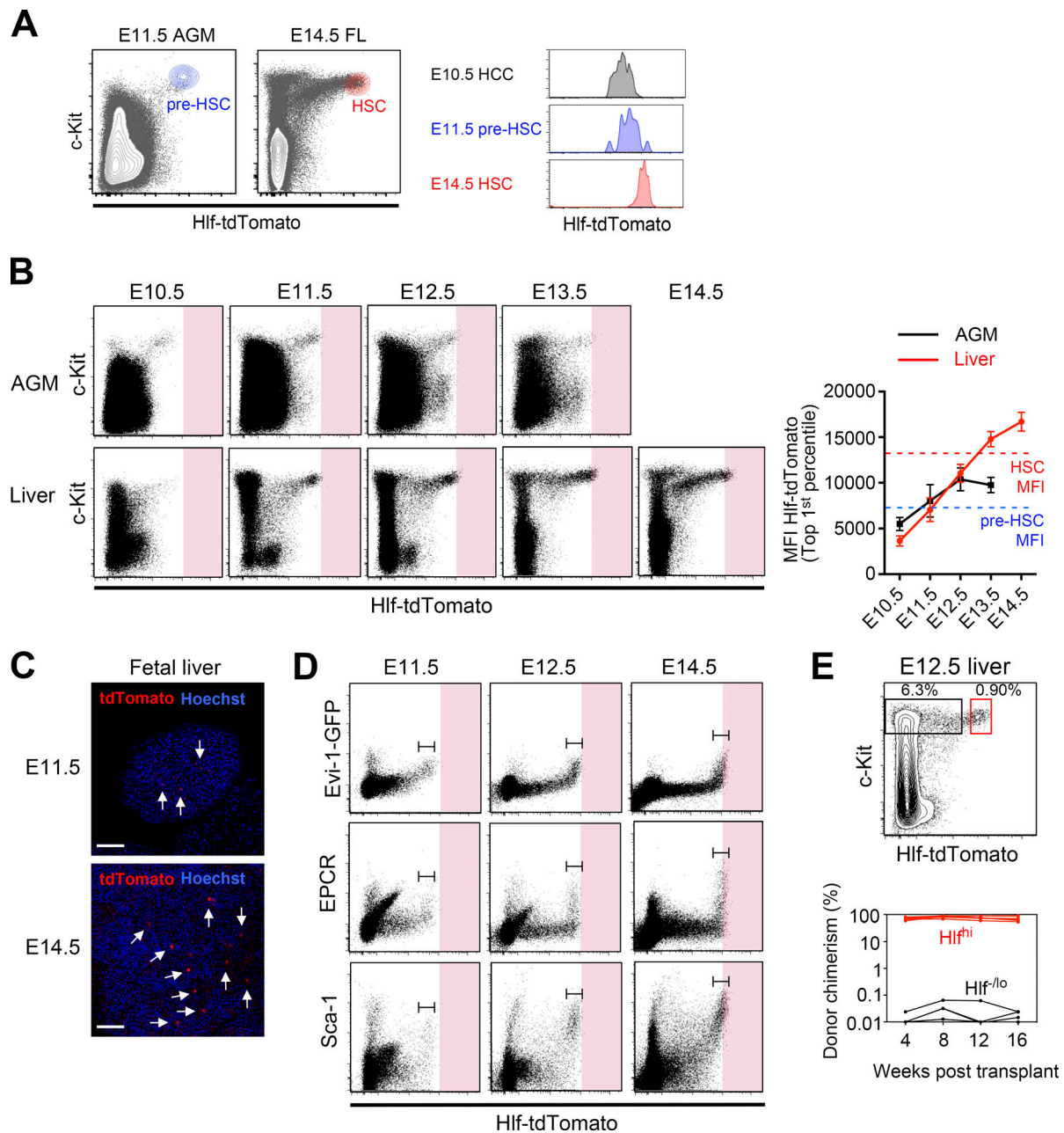


Figure 3. *Hlf* expression increases with HSC maturation. (A) Correlation between *Hlf* expression level and HSC maturation status. Left and middle: The location of pre-HSCs (CD31⁺CD45⁻CD41^{lo}c-Kit⁺EPCR^{hi}) and HSCs (CD150⁺CD48⁻ KSL) are shown in the Hlf-tdTomato/c-Kit plot. Right: *Hlf*-tdTomato expression in E10.5 HCCs (Hlf⁺c-Kit⁺), E11.5 pre-HSCs, and E14.5 HSCs. Data are representative of at least two independent experiments. FL, fetal liver; HCC, hematopoietic cluster cells. **(B)** *Hlf* expression in the AGM and fetal liver. Left: Flow cytometry analysis of cells from E10.5–14.5 embryos. Fluorescence intensity above E14.5 HSC mean fluorescence intensity (MFI) is indicated by the red-shaded area. Right: MFI of top first percentile Hlf⁺ cells ($n = 3-6$). Data are representative of at least two independent experiments. Error bars show means \pm SD. Representative gating strategy used to analyze MFI of top first percentile Hlf⁺c-Kit⁺ cells is shown in Fig. S3 C. **(C)** Confocal images of *Hlf*-tdTomato expression in the fetal liver at E11.5 and E14.5. Arrows indicate tdTomato⁺ cells. Data are representative of two independent experiments. Scale bar, 50 μ m. **(D)** HSC marker expression in Hlf^{hi} cells. Data are representative of at least two independent experiments. **(E)** Transplantation experiments. Top: Flow cytometry sorting of Hlf^{hi}c-Kit⁺ and Hlf^{lo/-}c-Kit⁺ cells from E12.5 *Hlf*^{tdTomato/+} fetal liver. Irradiated mice were transplanted with 5,000 Hlf^{hi} cells or 40,000 Hlf^{lo/-} cells. Bottom: Total donor reconstitution over the time course of transplantation ($n = 4-6$). Combined data are from two experiments.

showed that only 5% of c-Kit⁺ circulating cells were positive for *Hlf*-tdTomato (Figs. 2 C and 4 A), suggesting that *Hlf* expression does not mark EMPs. To verify this finding, we performed FACS analysis on cells from E9.5 embryos. We found that phenotypic EMPs (c-Kit⁺CD41⁺CD16/32⁺; McGrath et al., 2015a)

and their progenies (c-Kit⁻CD45⁺) at E9.5 were negative for *Hlf* (Fig. 4 B).

EMPs emerge from yolk sac endothelium through the formation of c-Kit⁺ hematopoietic clusters around E9 stage (Frame et al., 2016; Kasai et al., 2017). To determine whether nascent

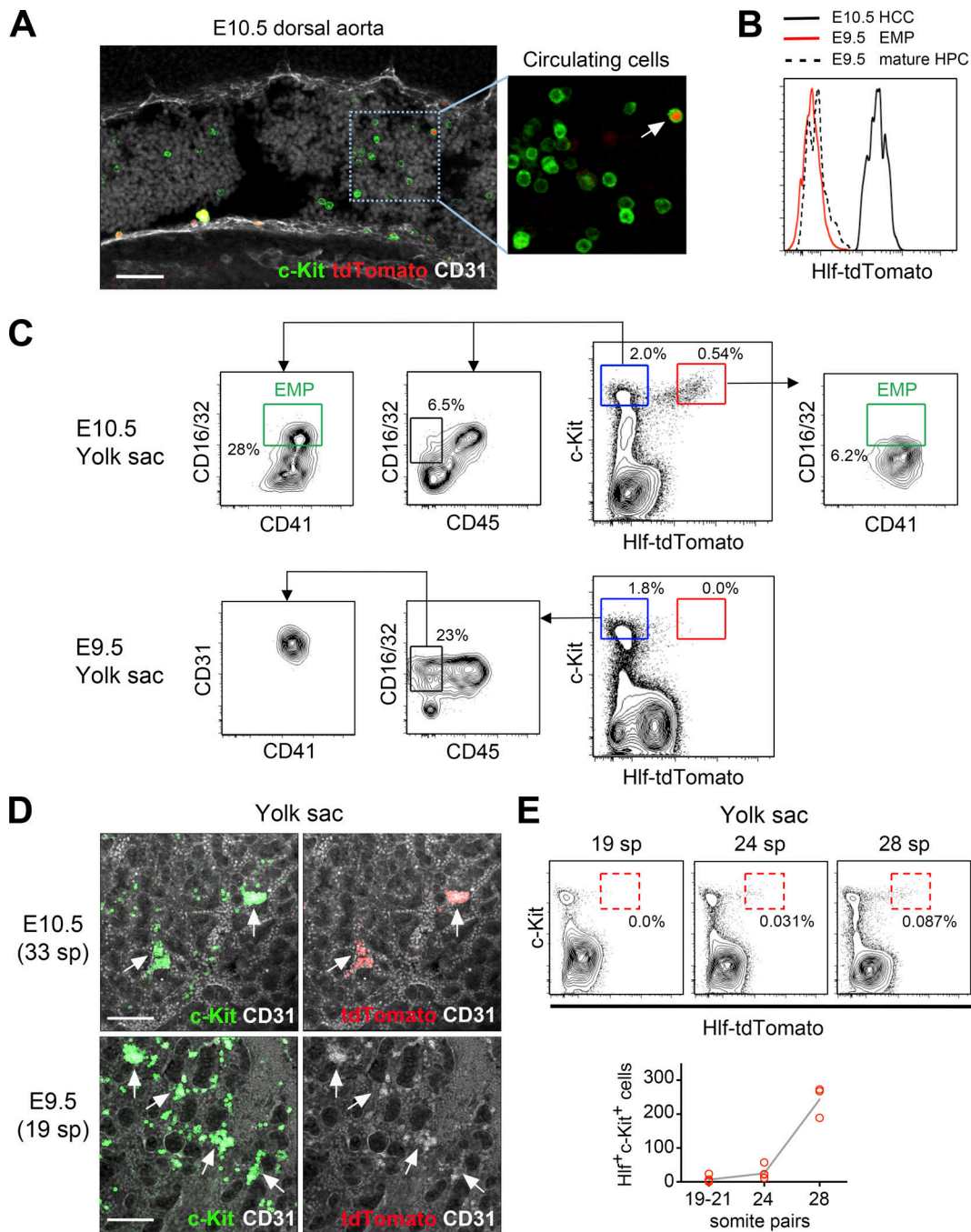


Figure 4. *Hlf* is not expressed in EMPs or hematopoietic clusters in E9.5 yolk sac. (A) *Hlf* expression in c-Kit⁺ circulating cells. Whole-mount immunostaining of E10.5 (37 sp) *Hlf^{tdTomato/+}* mouse for tdTomato (red), c-Kit (green), and CD31 (white) expression. Arrow indicates *Hlf*⁺c-Kit⁺ cell. Note that most c-Kit⁺ circulating cells are negative for tdTomato. Scale bar, 100 μm. **(B)** *Hlf*-tdTomato expression in EMPs (c-Kit⁺CD41⁺CD16/32⁺) and their progenies (c-Kit⁺CD45⁺). HCC, hematopoietic cluster cells; HPC, hematopoietic cells. Data are representative of at least four independent experiments. **(C)** Lack of *Hlf*⁺c-Kit⁺ subset in E9.5 yolk sac. Flow cytometry analysis of *Hlf*⁺c-Kit⁺ and *Hlf*⁻c-Kit⁺ cells in the yolk sac. Data are representative of at least four independent experiments. **(D)** *Hlf* expression in yolk sac hematopoietic clusters. Whole-mount immunostaining of *Hlf^{tdTomato/+}* yolk sacs at E10.5 (33 sp) and E9.5 (19 sp). Arrows indicate c-Kit⁺ hematopoietic clusters. Cell aggregates with >10 cells were defined as hematopoietic clusters. Scale bars, 100 μm. Data are representative of two independent experiments. **(E)** Numbers of *Hlf*⁺c-Kit⁺ cells in the yolk sac at different times of development. Numbers were calculated from flow cytometry data. Combined data are from three experiments. See also Fig. S4.

EMPs were *Hlf*⁻, we further analyzed the yolk sac at the 19–35 somite pair (sp) stage (E9–10). At E10.5, an *Hlf*⁺c-Kit⁺ cluster subset (0.54% ± 0.17%) with lymphoid potential was detected in the yolk sac (Fig. 4 C, red rectangle; see also Fig. S4, B–D). At this

stage, EMPs were enriched in the *Hlf*⁻c-Kit⁺ subset (1.8% ± 0.66%; Fig. 4 C, blue rectangle). However, at E9.5 (19–21 sp), the *Hlf*⁺c-Kit⁺ subset was almost absent (Fig. 4 C). Given that most EMPs are generated at E8–9 (Gomez Perdiguero et al., 2015),

these data imply that EMPs are generated through the formation of Hlf^{c-Kit} hematopoietic clusters. Indeed, a portion of the Hlf^{c-Kit} subset in the E9.5 yolk sac contains CD31⁺CD41⁺CD45⁻ cells (Fig. 4 C, black rectangle), representing a nascent phenotype of hematopoietic cluster cells (Yokomizo and Dzierzak, 2010; Frame et al., 2016).

Hlf is not expressed in hematopoietic clusters in the E9 yolk sac

Our FACS analysis results suggested that EMPs are generated through the formation of Hlf⁻ hematopoietic clusters. To confirm the existence of Hlf⁻ hematopoietic clusters in the yolk sac, we performed whole-mount immunostaining analysis. Consistent with the FACS data, c-Kit⁺ hematopoietic clusters expressed Hlf at E10.5 (33 and 34 sp), whereas c-Kit⁺ clusters at E9.5 (19 sp) did not (Figs. 4 D and S4 E). Hlf⁻ cells were rarely observed within E10.5 Hlf⁺ hematopoietic clusters (Fig. 2, C and E; and Fig. 4 D). These data indicate that c-Kit⁺ hematopoietic clusters are subdivided into Hlf⁺ and Hlf⁻ types, and also suggest that there is a developmental switch from an Hlf⁻ to Hlf⁺ cluster-producing phase between E9 and E10.

To determine the precise stage of Hlf⁺ hematopoietic cluster emergence, we analyzed the E9 to E10 stages in detail. At 19–21 sp, we observed 0–24 Hlf⁺c-Kit⁺ cells in the yolk sac per embryo (Fig. 4 E), indicating that Hlf⁺ hematopoietic clusters emerge around the 20-sp stage. Collectively, these data suggest that the developmental pathway for EMPs is negative for Hlf.

HSC program is activated in Hlf⁺ hematopoietic clusters

To obtain mechanistic insight into HSC specification, we compared the gene expression profiles between Hlf⁺ and Hlf⁻ hematopoietic clusters. Hlf⁺ and Hlf⁻ nascent hematopoietic cluster cells (c-Kit⁺CD45⁻; Yokomizo and Dzierzak, 2010) were isolated from E10.5 (35 and 36 sp) caudal half and E9.5 (18–20 sp) yolk sac, respectively, and were subjected to RNA sequencing (RNA-seq) analysis (Figs. 5 A and S5, A and B). We identified 872 genes up-regulated (more than a twofold change) and 318 genes down-regulated in the Hlf⁺ fraction (Figs. 5 B and S5, C–F). Consistent with the specific marking of HSCs by Hlf expression, gene set enrichment analysis (GSEA) indicated that HSC and EMP signatures were highly enriched in Hlf⁺ and Hlf⁻ fractions, respectively (Fig. 5 C). In contrast, analysis with progenitors (HSPCs) and differentiated progeny (erythroid and myeloid) signatures showed similarity between the two fractions (Figs. 5 C and S5 D), suggesting that the Hlf⁻ fraction has characteristics of hematopoietic progenitors but lacks an activation of the HSC program. Accordingly, HSC genes (*Hlf*, *Mecom*, *Procr*, *Hoxa9*, and *Vwf*) were specifically detected in the Hlf⁺ fraction (Fig. 5 D). In addition, Hlf⁺ cluster cells expressed a broad range of Hox cluster genes, partly consistent with a previous report that HOXA genes are expressed in human AGM, fetal liver HSPCs, and AGM-like hematopoietic cells induced from human embryonic stem (ES) cells (Dou et al., 2016; Ng et al., 2016). GSEA also revealed enrichment of Notch, bone morphogenetic protein, and Wnt signaling genes in the Hlf⁺ fraction (Fig. S5 D), in line with their positive effects on HSC generation (Hadland et al., 2004; Sturgeon et al., 2014; Crisan et al., 2016). Among HSPC-related

genes, factors with known roles in EHT (*Runx1*, *Gata2*, *Tali*, *Meis1*, and *Racl*; Azcoitia et al., 2005; Ghiaur et al., 2008; Chen et al., 2009; de Pater et al., 2013; Zhen et al., 2013) were comparably expressed in both fractions (Fig. 5 D), probably reflecting the common program for EHT progression in the yolk sac and the major arteries. Together, our RNA-seq data support the notion that acquisition of the HSC or EMP fate takes place at the formation of hematopoietic clusters or earlier.

Evi-1/Hlf axis regulates HSC maturation

Our RNA-seq analysis suggested that HSC-specifying genes can be distinguished from other HSPC-related genes (Fig. 5 D). One of the candidate HSC-specifying genes is *Mecom* (*Evi-1*). Immunological Genome Project (<https://www.immgen.org>) data also suggests that *Mecom* is most closely correlated with *Hlf* within the HSPC gene network. Given that functional HSCs are absent in *Evi-1*-deficient embryos (Goyama et al., 2008), we predicted that *Evi-1* is involved in preHSC to HSC maturation but not in EMP formation or EHT progression. To clarify the function of *Evi-1* in embryonic hematopoiesis and the relationship between *Evi-1* and *Hlf*, we crossed Hlf^{tdTomato/+} mice with *Evi-1* mutant mice. As expected, *Evi-1*^{-/-} embryos at E10.5 had a normal Hlf^{c-Kit} EMP-enriched fraction (Fig. 6 A), and an analysis of E9.5 yolk sac confirmed absence of *Evi-1* expression in EMPs and intact EMP formation in *Evi-1*^{-/-} embryos (Fig. 6, B and C). In contrast to Hlf^{c-Kit} EMP-enriched cells, there were obviously fewer Hlf^{c-Kit} hematopoietic cluster cells in *Evi-1*^{-/-} embryos at E10.5 (Fig. 6 A).

We next performed whole-mount immunostaining analysis to investigate whether hematopoietic clusters formed in *Evi-1*^{-/-} embryos. c-Kit⁺ hematopoietic clusters formed normally in the *Evi-1*^{-/-} dorsal aorta, but there was a decrease in Hlf-tdTomato expression in the hematopoietic clusters (Fig. 6, D and E), indicating that *Evi-1* is not required for EHT but regulates Hlf expression in hematopoietic clusters. Because Hlf expression is indicative of HSC maturation status (Fig. 3), these data also suggest that *Evi-1* is involved in HSC maturation. To examine this, we next analyzed E12.5 fetal liver of the *Evi-1*^{-/-}::Hlf^{tdTomato/+} mouse. An up-regulation in Hlf was observed in *Evi-1*^{+/+} fetal liver cells but not in *Evi-1*^{-/-} cells (Fig. 6 F). In addition, Hlf⁺EPCR⁺ and Hlf⁺Sca-1⁺ subsets did not emerge in *Evi-1*^{-/-} fetal liver (Fig. 6 G). These data support a role for *Evi-1* in the maturation of preHSCs into HSCs and suggest that the Hlf-tdTomato reporter system is a useful tool for dissecting HSC-dependent and -independent lineage development in the mouse embryo.

Myb regulates EMP maintenance or expansion

It remains controversial how Myb is involved in the formation of HSC-independent hematopoiesis (Schulz et al., 2012; Hoeffel et al., 2015; McGrath et al., 2015b; Perdiguero and Geissmann, 2016). Although some c-Kit⁺ cells can be detected in the Myb-deficient embryo (Schulz et al., 2012), the developmental origin of those c-Kit⁺ cells is unclear. To explore the function of Myb in definitive hematopoiesis, we crossed the Myb mutant mouse with the Hlf^{tdTomato/+} reporter mouse. At E10.5, the Hlf⁺ hematopoietic cluster subset (Hlf⁺c-Kit⁺) was normally formed in the Myb^{-/-} embryos (Fig. 7 A). Consistently, whole-mount immunostaining analysis also showed normal formation of c-Kit⁺

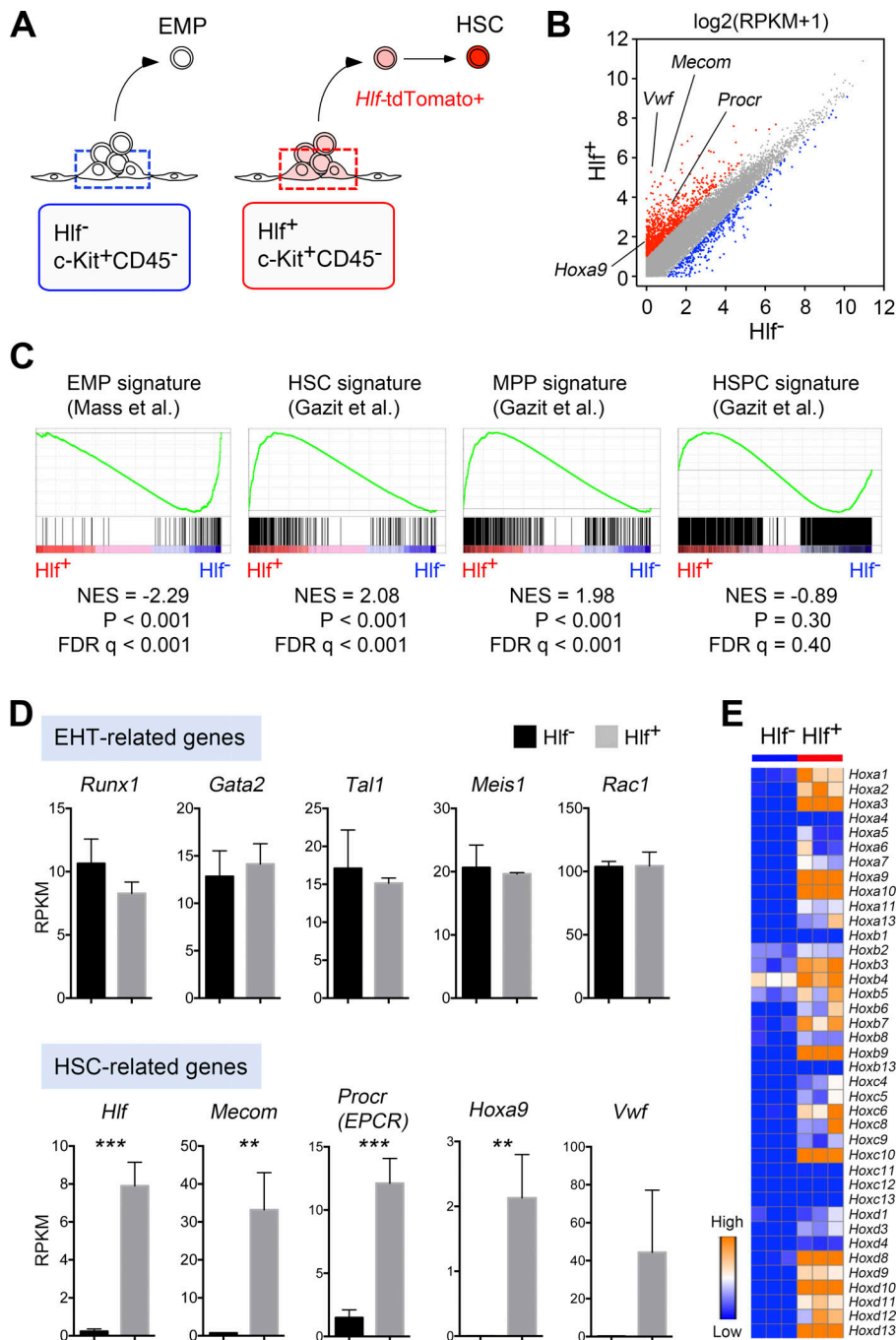


Figure 5. Transcriptome analysis of *Hlf*⁺ and *Hlf*⁻ nascent hematopoietic cluster cells. (A) Schematic representation of isolated populations for RNA-seq analysis. *Hlf*⁻*c-Kit*⁺*CD45*⁻ and *Hlf*⁺*c-Kit*⁺*CD45*⁻ nascent hematopoietic cluster cells (dotted squares) were sorted from E9.5 (18–20 sp) yolk sac and E10.5 caudal half (35 and 36 sp), respectively. **(B)** Scatter plot comparing gene expression between *Hlf*⁻*c-Kit*⁺*CD45*⁻ and *Hlf*⁺*c-Kit*⁺*CD45*⁻ cells. Genes up-regulated and down-regulated more than twofold are plotted in red and blue, respectively. RNA-seq data are generated from three independent sorts. **(C)** GSEA of *Hlf*⁺*c-Kit*⁺*CD45*⁻ subset compared with *Hlf*⁻*c-Kit*⁺*CD45*⁻ subset for EMP, HSC, and progenitor signatures. NES, normalized enrichment score; FDR, false discovery rate; MPP, multipotential progenitors. **(D)** Expression of EHT and HSC-related genes in *Hlf*⁻*c-Kit*⁺*CD45*⁻ and *Hlf*⁺*c-Kit*⁺*CD45*⁻ cells, presented as reads per kilobase of transcript per million mapped reads (RPKM). Error bars show means ± SD. *, *P* < 0.05; **, *P* < 0.01; ***, *P* < 0.001 (unpaired two-tailed Student's *t* test). **(E)** Heatmap showing Hox cluster gene expression in *Hlf*⁺*c-Kit*⁺*CD45*⁻ and *Hlf*⁻*c-Kit*⁺*CD45*⁻ cells. See also Fig. S5.

aortic clusters in *Myb*^{-/-} embryos (Fig. 7, B and C), indicating that *Myb* is not required for *Hlf*⁺ hematopoietic cluster formation. In contrast to the *Hlf*⁺*c-Kit*⁺ subset, there was a severe decrease in the EMP-enriched *Hlf*⁻*c-Kit*⁺ subset in E10.5 *Myb*^{-/-} embryos (Fig. 7 A). These results, combined with the *Evi-1*^{-/-} analysis in Fig. 6 A, indicate that the formation of *Hlf*⁺*c-Kit*⁺ and *Hlf*⁻*c-Kit*⁺ subsets is uncoupled. The near absence of EMPs in the E10.5 *Myb*^{-/-} embryo was confirmed by an analysis of the yolk sac and the embryo proper (Fig. 7 D). In agreement with this data, *c-Kit*⁺ circulating cells, which include numerous EMPs, were rarely observed in the *Myb*^{-/-} dorsal aorta at E10.5 (Fig. 7 E).

Given that *Myb* is not expressed in hemogenic endothelium (Fig. 1 A; Swiers et al., 2013), it is likely that *Myb* is involved in

EMP maintenance or expansion but not in EMP formation from hemogenic endothelium. To examine this, we analyzed the yolk sac at E9, which is the major site and stage for EMP formation. Although we observed a slight reduction in the numbers of EMPs (*P* = 0.02), substantial numbers of EMPs were still formed in the *Myb*^{-/-} embryos (Fig. 7 F). Taken together, these data indicate that *Myb* is required for EMP maintenance or expansion but not for formation.

Discussion

A detailed analysis of HSC specification has been hampered by the coexistence of HSC-independent lineages, such as EMPs,

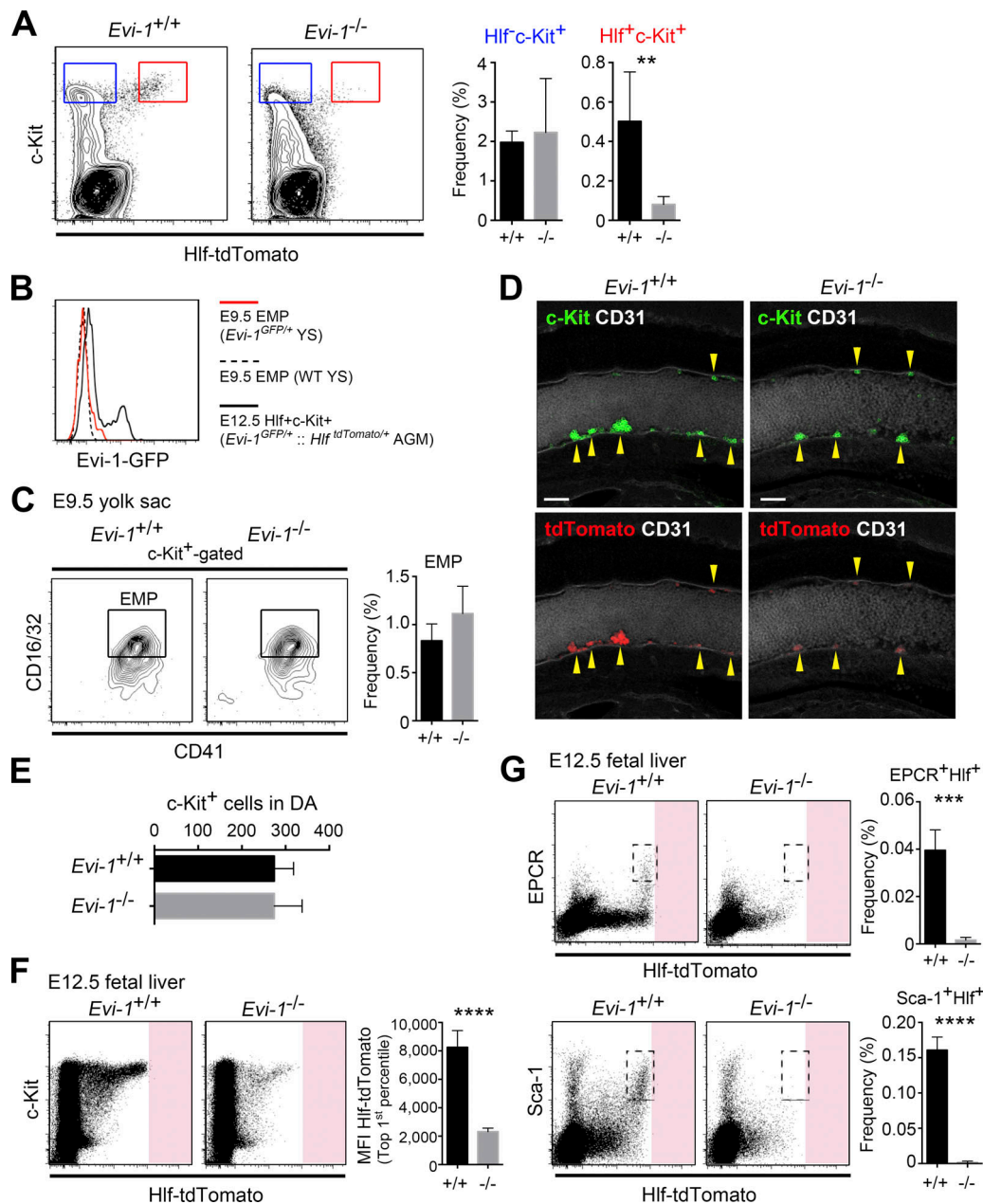


Figure 6. *Evi-1* is required for HSC maturation but not for EMP formation. (A) Specific decrease in the Hlf⁺c-Kit⁺ subset in the *Evi-1*^{-/-} embryo. Left: Representative flow cytometric plot. Right: Frequency of Hlf⁺c-Kit⁺ and Hlf⁻c-Kit⁺ subsets. *Evi-1*^{+/+} (*n* = 5, 32–36 sp). *Evi-1*^{-/-} (*n* = 7, 32–36 sp). Four independent experiments. (B) *Evi-1*-GFP expression in EMPs. Data are representative of at least two independent experiments. YS, yolk sac. (C) EMPs in the E9.5 yolk sac. Left: Representative flow cytometric plot. Right: Frequency of EMP subset. *Evi-1*^{+/+} (*n* = 4, 17–20 sp). *Evi-1*^{-/-} (*n* = 3, 16–21 sp). Two independent experiments. (D) Whole-mount immunostaining of *Evi-1*^{+/+}::*Hlf*^{tdTomato/+} and *Evi-1*^{-/-}::*Hlf*^{tdTomato/+} embryos. *Evi-1*^{+/+} (35 sp). *Evi-1*^{-/-} (35 sp). Yellow arrowheads indicate c-Kit⁺ hematopoietic clusters. Scale bars, 50 μ m. (E) Number of c-Kit⁺ cells localized in the middle segment of dorsal aorta. Middle segment is seven somite lengths (Yokomizo and Dzierzak, 2010). *Evi-1*^{+/+} (*n* = 3, 38–39 sp). *Evi-1*^{-/-} (*n* = 3, 38–40 sp). Three independent experiments. DA, dorsal aorta. (F) Decrease in Hlf-tdTomato expression in E12.5 *Evi-1*^{-/-} fetal liver. Left: Representative flow cytometric plot. Right: MFI of top first percentile Hlf⁺ cells. *Evi-1*^{+/+} (*n* = 4). *Evi-1*^{-/-} (*n* = 4). Two independent experiments. (G) Decrease in HSC marker expression in E12.5 *Evi-1*^{-/-} fetal liver. Left: Representative flow cytometric plot. Right: Frequency of EPCR⁺Hlf⁺ and Sca-1⁺Hlf⁺ subsets. *Evi-1*^{+/+} (*n* = 4). *Evi-1*^{-/-} (*n* = 4). Two independent experiments. Error bars show means \pm SD. **, *P* < 0.01; ***, *P* < 0.001; ****, *P* < 0.0001 (unpaired two-tailed Student's *t* test).

which have surface markers similar to embryonic HSCs and are abundantly present in the midgestation phase of embryogenesis (Dzierzak and Bigas, 2018). Here, we demonstrate that nascent HSCs and EMPs are distinguished by the expression of *Hlf*, and this knowledge enables us to access embryonic HSCs and their

precursors more easily. Using this new reporter mouse combined with RNA-seq and confocal imaging analyses, we demonstrate that Hlf⁺ and Hlf⁻ hematopoietic clusters contribute to HSCs and EMPs, respectively. Moreover, HSC specification is already activated within Hlf⁺ nascent hematopoietic clusters.

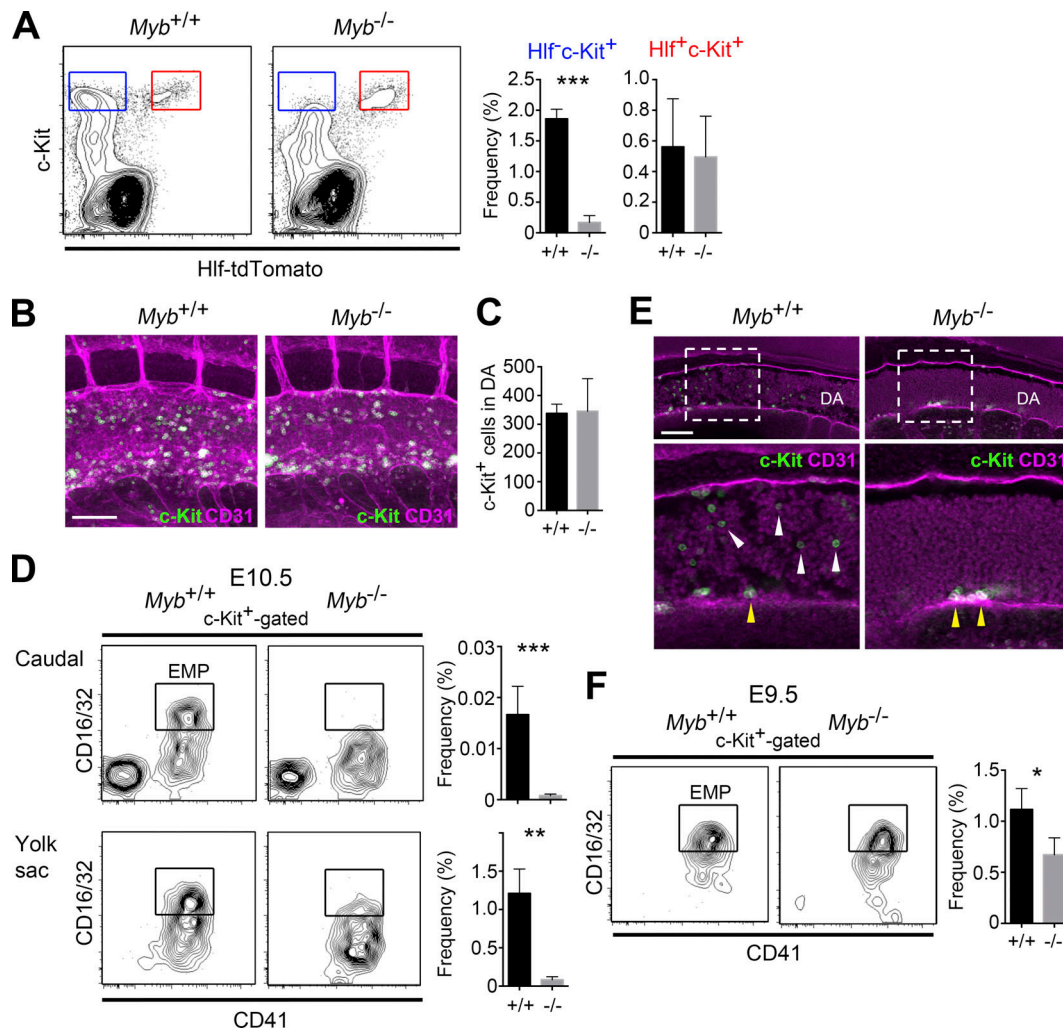


Figure 7. *Myb* is required for EMP but not for *Hlf*⁺ hematopoietic cluster formation. (A) Specific decrease in the *Hlf*⁺*c-Kit*⁺ subset in the *Myb*^{-/-} embryo. Left: Representative flow cytometric plot. Right: Frequency of *Hlf*⁺*c-Kit*⁺ and *Hlf*⁺*c-Kit*⁺ subsets. *Myb*^{+/+} (*n* = 3, 33–36 sp). *Myb*^{-/-} (*n* = 3, 33–36 sp). Two independent experiments. (B) Whole-mount immunostaining of *Myb*^{+/+} and *Myb*^{-/-} embryos for *c-Kit* (green) and CD31 (magenta) expression. 3D view. *Myb*^{+/+} (36 sp). *Myb*^{-/-} (35 sp). Scale bar, 100 μ m. (C) Number of *c-Kit*⁺ cells localized in the middle segment of dorsal aorta (DA). Middle segment is seven somite lengths (Yokomizo and Dzierzak, 2010). *Myb*^{+/+} (*n* = 3, 33–35 sp). *Myb*^{-/-} (*n* = 3, 33 and 34 sp). Two independent experiments. (D) EMPs in the E10.5 yolk sac. Left: Representative flow cytometric plot. Right: Frequency of EMP subset. *Myb*^{+/+} (*n* = 4, 35 and 36 sp). *Myb*^{-/-} (*n* = 4, 35 and 36 sp). Two independent experiments. (E) Whole-mount immunostaining of *Myb*^{+/+} and *Myb*^{-/-} embryos for *c-Kit* (green) and CD31 (magenta) expression. Confocal section. Yellow arrowheads indicate *c-Kit*⁺ hematopoietic clusters. Note that *c-Kit*⁺ circulating cells (white arrowheads in *Myb*^{+/+} dorsal aorta) are not observed in the *Myb*^{-/-} dorsal aorta. *Myb*^{+/+} (36 sp). *Myb*^{-/-} (35 sp). Scale bar, 100 μ m. (F) EMPs in the E9.5 yolk sac. Left: Representative flow cytometric plot. Right: Frequency of EMP subset. *Myb*^{+/+} (*n* = 5, 17–22 sp). *Myb*^{-/-} (*n* = 3, 18–22 sp). Three independent experiments. Error bars show means \pm SD. *, *P* < 0.05; **, *P* < 0.01; ***, *P* < 0.001 (unpaired two-tailed Student's *t* test).

These results strongly suggest that HSCs and EMPs are generated from distinct populations of hemogenic endothelium. This inference is consistent with the model proposed in a previous genetic study, where uncoupling formation of HSCs and EMPs was seen in *Cbfb*^{-/-} mice rescued by *Ly6a-Cbfb* or *Tek-Cbfb* transgenes (Chen et al., 2011).

RNA-seq data showed that EHT-related genes, *Runx1*, *Gata2*, *Tal1*, *Meis1*, and *Racl*, were comparably expressed in *Hlf*⁺ and *Hlf*⁻ subsets, probably reflecting the existence of common EHT machinery in HSC- and EMP-producing cluster formation. Moreover, we did not observe significant differences in the gene signatures of progenitor, erythroid, or myeloid genes between the *Hlf*⁺ and *Hlf*⁻ subsets, indicating that progenitor features are

common to both subsets. We speculate that these progenitor features are the default state of nascent hematopoietic cells, with supplementary HSC program activation through *Hlf* expression endowing the cells with stem cell properties. Consistently, a recent study showed that polycomb group protein *Ezh1* represses the HSC program, including *Hlf* expression, before the emergence of HSCs (Vo et al., 2018).

In this study, we identified *Evi-1* as a factor specific to HSC development. In *Evi-1*-deficient embryos, *Hlf* expression was decreased but not completely lost, indicating that *Evi-1* is an upstream regulator of *Hlf*. Given that *Mecom* is most closely correlated with *Hlf* in the HSPC gene network (Immunological Genome Project database), *Evi-1* may directly regulate the *Hlf*

gene. In contrast to *Evi-1*, it seems that *Hlf* is dispensable for HSC generation, as adult *Hlf*-deficient mice exhibited normal steady-state hematopoiesis (Komorowska et al., 2017). However, we speculate that *Hlf* is involved in the transcriptional circuitry of HSC specification for the following reasons. First, over-expression of *Hlf* influences the fate of stem cells or progenitors. For example, *Hlf*, together with five other transcription factors, can transform committed blood progenitors into functional HSCs (Riddell et al., 2014); this suggests that *Hlf* can induce stemness. Second, there may be a functional redundancy with other PAR-bZip family proteins (Dbp and Tef) or CCAAT/enhancer binding proteins, which share a similar binding motif with *Hlf* (Wahlestedt et al., 2017).

Interestingly, we found that *Hlf*⁺ hematopoietic clusters are also localized in the yolk sac. These cells first appear between E9 and E10 and show a similar surface marker phenotype with intra-aortic *Hlf*⁺ hematopoietic clusters, which express CD41, CD31, and EPCR (data not shown). Recently, Yzaguirre and Speck (2016) reported that progenitors with lymphoid potential are enriched in *Ly-6a*-GFP⁺ population in the yolk sac. Since both the lymphoid potential of *Ly-6a*-GFP⁺ population and *Hlf*⁺ cells in the yolk sac emerge at ~E10, and the expression level of *Sca-1*, which is encoded by *Ly-6a* gene, correlates with that of *Hlf* (Fig. 3 D), it is likely that *Hlf*⁺ hematopoietic clusters in the yolk sac contain *Ly6a*-GFP⁺ cells. Furthermore, a Lyve1-based lineage tracing study showed that a subset of adult HSCs are generated from yolk sac hemogenic endothelium (Lee et al., 2016). We speculate that yolk sac-derived HSCs may be generated through the formation of *Hlf*⁺ hematopoietic clusters. Studies with lineage tracing of yolk sac *Hlf*⁺ cells are required to prove this hypothesis.

The AGM and fetal liver are proposed sites for pre-HSC to HSC maturation (Taoudi et al., 2008; Kieusseian et al., 2012; Rytsov et al., 2016). We showed that *Hlf* expression levels correlate well with HSC maturation status. Moreover, we observed a continuous increase in *Hlf* expression in the fetal liver but not in the AGM, suggesting that the fetal liver is the major site for HSC maturation. Others have reported drastic increases (28–176-fold) in HSC number in fetal liver between E11 and E12 (Kumaravelu et al., 2002; Gekas et al., 2005). This may be explained by the simultaneous maturation of pre-HSCs in the fetal liver during this period, rather than by HSC expansion through rapid symmetric divisions.

The generation of engraftable HSCs from pluripotent stem cells is a long-standing challenge in regenerative medicine. The current typical culture conditions mimic yolk sac-phase hematopoiesis and result in the preferential generation of EMPs from pluripotent stem cells (McGrath et al., 2015a). A recent study has improved the culture conditions for human ES cells by stimulating retinoic acid signaling or modulating WNT and ACTIVIN signaling, leading to AGM-like gene expression in induced hematopoietic cells (Dou et al., 2016; Ng et al., 2016). The study also emphasized that *HOXA* expression is a landmark of AGM-like hematopoiesis (Ng et al., 2016). Consistent with those findings, we demonstrated that *Hox* cluster genes are specifically expressed in *Hlf*⁺*c-Kit*⁺ nascent hematopoietic cells. Therefore, similar to *HOXA* gene expression, *Hlf* expression could serve as a

landmark of pre-HSC emergence. In addition to the detection of preHSC emergence, the *Hlf*-tdTomato reporter can monitor the maturation status of HSCs. Therefore, we believe that the *Hlf*-tdTomato reporter ES cell line is suitable for optimizing culture conditions for inducing both preHSC emergence and its maturation in vitro.

Materials and methods

Mice and embryos

All mice were on the C57BL/6 background. *Runx1-GFP* (*eR1-GFP*), *Evi-1^{GFP/+}*, *Evi-1^{+/-}*, *Myb^{GFP/+}*, and *Myb^{+/-}* mice were described previously (Mucenski et al., 1991; Goyama et al., 2008; Ng et al., 2010; Kataoka et al., 2011; Sakamoto et al., 2015). C57BL/6-Ly5.2 (Ly5.2) and C57BL/6-Ly5.1 (Ly5.1) mice were purchased from Japan SLC and Sankyo-Lab Service, respectively. Embryos were generated by timed matings and were staged according to embryonic day, somite pairs, and Thelie criteria (<http://www.emouseatlas.org/emap/home.html>). For the bone marrow analysis, 8–13-wk-old mice were used. All animal experiments were performed in accordance with institutional guidelines and were approved by the Institutional Animal Care and Use Committee of the National University of Singapore; the Ethics Committees on Animal Experimentation, Juntendo University; and the Animal Care and Use Committee of Kumamoto University.

Generation of the *Hlf^{tdTomato/+}* reporter mouse

To generate the targeting vector, the right and left arms (1,393 and 815 bp, respectively) were cloned from mouse genomic DNA (Clontech). A cassette bearing a T2A/tdTomato/BGHpolyA was inserted before the endogenous terminal codon within exon 4.

Oocytes were collected from C57BL/6J female mice (Charles River Laboratories Japan) superovulated with 10 IU of pregnant mare's serum gonadotropin (Peamex; Sankyo Lifetech) followed by 10 IU of human chorionic gonadotropin (hCG; Sigma-Aldrich) ~48 h later. The females were sacrificed 14 h after the hCG injection to collect metaphase II oocytes. The complex of oocytes and cumulus cells was released from oviducts into 0.1% hyaluronidase (Sigma-Aldrich) in Hepes-mCZB for 2 min at 37°C to disperse cumulus cells. The cumulus-free oocytes were washed and maintained in modified Whitten's medium at 37°C in 5% CO₂ air atmosphere until use. Cauda epididymides were removed from C57BL/6J males (Charles River Laboratories Japan). The epididymides were excised with a pair of fine scissors and compressed with forceps to release the dense mass of spermatozoa into 1 ml of Hepes-mCZB in 1.5-ml microtubes (96.7246.9.01; Treff). The spermatozoa dispersed in the microtubes for 5 min at 37°C. After gently pipetting, sperm-containing microtubes were then placed on ice until use. Sperm suspensions (10⁶ in 29 μl) were mixed with 1 μl of targeting vector solution (253 ng/μl) and clustered regularly interspaced short palindromic repeat (CRISPR) vector pX330 expressing Cas9 and *Hlf*-specific single guide RNA (5'-AGGCACGGGCCCTGTAAAGA-3'; 192 ng/μl) and incubated at ambient temperature for 2 min. Intracytoplasmic sperm injection (ICSI) was performed according to the method of Kimura and Yanagimachi (1995) with slight

modifications. 5 μ l of the mixture of sperm-targeting vector and CRISPR vector were diluted with 10 μ l of Hepes-mCZB containing 12% polyvinylpyrrolidone (*M_n*, 360,000; Sigma-Aldrich) before use. The ICSI dish contained a drop of Hepes-mCZB, a sperm-targeting vector, CRISPR vector drop, and a Hepes-mCZB/12% polyvinylpyrrolidone needle-cleaning drop. Injections were performed by micromanipulators (Leica) with a PMM-150 FU piezo-impact drive unit (Prime Tech) using a blunt-ended, mercury-containing injection pipette with \sim 6 μ m inner diameter. A single spermatozoon was drawn, tail first, into the injection pipette and moved back and forth until the head-midpiece junction was at the opening of the injection pipette. The head was separated from the midpiece by applying one or more piezo pulses. After discarding the midpiece and tail, the head was redrawn into the pipette and injected immediately into an oocyte. Sperm-injected oocytes were washed with modified Whitten's medium and cultured in 20- μ l drops of the same medium covered with mineral oil at 37°C in 5% CO₂ in air. The oocytes were examined \sim 6 h after ICSI for survival and activation. The oocytes with two well-developed pronuclei were recorded at 7 h after ICSI to assess fertilizing ability. Two-cell-stage embryos, cultured for \sim 24 h and developed from oocytes fertilized by ICSI, were transferred to oviducts of the pseudo-pregnant ICR recipient females (Charles River Laboratories Japan) that were mated to vasectomized ICR male mice (Charles River Laboratories Japan). The embryo transfer to the pseudo-pregnant females was performed on the day that the vaginal plug was detected.

Generated *Hlf^{tdTomato/+}* reporter mice were genotyped by PCR amplification using the following primers: forward (5'-TAGTTGCCAGCCATCTGTTG-3') and reverse (5'-TCCCATTCTGAGATACACCAGTG-3'). The annealing location of the reverse primer was designed to be outside the homology arm. Wild-type *Hlf* allele was detected by PCR using forward (5'-CAGGAGGTGGCTGATTTAAG-3') and reverse (5'-TCCCATTCTGAGATACACCAGTG-3') primers.

Whole-mount immunostaining of embryos

Whole-mount immunostaining was performed as described previously (Yokomizo et al., 2012). Briefly, embryos were fixed for 20 to 30 min in 2% paraformaldehyde diluted in PBS on ice and dehydrated in graded concentrations of methanol/PBS (50%, 100%; 10 min each). For staining around the dorsal aorta region, the yolk sac, head, limb buds, and lateral body wall were removed in 100% methanol. When using streptavidin/biotin reaction, endogenous biotin activity was blocked with streptavidin/biotin blocking kit (Vector Laboratories) following the manufacturer's instructions. After preincubation with PBS-MT (PBS containing 0.4% Triton X-100 and 1% skim milk) for \geq 1 h, samples were incubated overnight with primary antibody diluted in PBS-MT and washed three times in PBS-MT throughout the next day (2–3 h per wash). Secondary antibody was diluted in PBS-MT, and samples were incubated overnight. Primary antibodies used were for c-Kit (rat, 2B8; BD Biosciences), biotinylated CD31 (rat, MEC 13.3; BD Biosciences), c-Kit (goat; R&D Systems), GFP (rabbit; MBL), RFP (rabbit; MBL), and RFP (rabbit; Rockland Immunochemicals). Secondary

antibodies (or streptavidin conjugates) were goat anti-rat IgG-Alexa Fluor 555 (Invitrogen), goat anti-rabbit IgG-Alexa Fluor 647 (Invitrogen), donkey anti-rat IgG-Alexa Fluor 488 (Jackson ImmunoResearch), donkey anti-goat IgG-cyanine 3 [Cy3] (Jackson ImmunoResearch), and Cy3-streptavidin (Jackson ImmunoResearch). Nuclei were visualized with Hoechst 33258 (Invitrogen).

Whole-mount immunostaining of bone marrows

Freshly dissected femurs were fixed in cold paraformaldehyde-lysine-periodate buffer for 8 h at 4°C, rehydrated in 30% sucrose solution for 48 h, and snap frozen in optimum cutting temperature compound (Tissue Tek). Frozen femurs were sectioned using a Leica cryostat until the bone marrow cavity was exposed along the longitudinal axis. This procedure was repeated on the opposite side. The bone samples were washed with PBS and blocked overnight at 4°C in blocking solution (0.2% Triton X-100, 1% BSA, and 10% donkey serum in PBS). The bone marrow slices were stained with anti-laminin (rabbit; Sigma-Aldrich), Alexa Fluor 488-conjugated anti-Sca-1 (rat, E13-161.7; BioLegend), anti-c-Kit (goat; R&D Systems), and anti-RFP (chicken; Rockland Immunochemicals) overnight at 4°C in blocking solution, washed overnight in PBS, and stained with donkey anti-rabbit IgG-Alexa Fluor 488 (Jackson ImmunoResearch), donkey anti-goat IgG (heavy and light chains [H+L])–Alexa Fluor 647 (Jackson ImmunoResearch), and donkey anti-chicken IgY (IgG; H+L)-Cy3 (Jackson ImmunoResearch).

Confocal microscopy and image analysis

Immunostained caudal half, yolk sac, and fetal livers were mounted in a 1:2 mix of benzyl alcohol and benzyl benzoate to increase the transparency of tissues and were analyzed with a confocal microscope (Olympus FV-1200 equipped with gallium arsenide phosphide photomultiplier tube detectors, UPLSAPO 20 \times /NA 0.75). Immunostained bone marrow samples were incubated overnight in RapiClear1.52 (SunJin Lab Funakoshi). Samples were mounted on glass slides and analyzed with a confocal microscope (Leica SP8, HC PL APO CS2 20 \times /0.75 DRY). Three-dimensional (3D) reconstructions were generated from z-stacks with Olympus FluoView software or Imaris software (Bitplane).

Cell preparation and flow cytometry

Single-cell suspensions were prepared by treating tissues with collagenase (0.125% in PBS, 10% FCS, and 1% penicillin/streptomycin) for 1 h at 37°C. Bone marrow cells were prepared by crushing the bones using a mortar. Cell number was counted using a TC20 automated cell counter (Bio-Rad). Cells were stained with fluorescence-conjugated antibodies: c-Kit (2B8, BV421; BioLegend), c-Kit (2B8, PE-Cy7; BD Biosciences), c-Kit (2B8, allophycocyanin [APC]; BD Bioscience), CD31 (MEC13.3, FITC; BD Biosciences), SSEA-1 (MC-480, PE; eBiosciences), SSEA-1 (MC-480, V405; BD Biosciences), CD45 (30-F11, peridinin-chlorophyll protein [PerCP]-Cy5.5; BD Biosciences), CD45 (30-F11, PerCP-Cy5.5; BioLegend), CD45 (30-F11, BV510; BD Biosciences), Sca-1 (D7, PerCP-Cy5.5; eBioscience), Sca-1 (D7, PE-Cy7; BioLegend), Sca-1 (D7, APC-Cy7; BioLegend), CD150

(TC15-12F12.2, APC; BioLegend), CD150 (TC15-12F12.2, Alexa Fluor 488; BioLegend), CD48 (HM48-1, FITC; BD Biosciences), CD48 (HM48-1, APC-Cy7; BioLegend), CD41 (MWRReg30, PerCP-eFluor710; eBioscience), CD16/32 (93, APC; BioLegend), EPCR (eBio1560, APC; eBioscience), Ter119 (TER-119, biotin; BD Biosciences), Ter119 (TER-119, PE; BD Biosciences), CD3e (145-2C11, biotin; BD Biosciences), CD3e (145-2C11, PE; BD Biosciences), CD4 (GK1.5, biotin; BD Biosciences), CD4 (GK1.5, PE; BD Biosciences), CD8a (53-6.7, biotin; BD Biosciences), CD8a (53-6.7, PE; BD Biosciences), B220 (RA3-6B2, biotin; BD Biosciences), B220 (RA3-6B2, PE; BD Biosciences), Gr-1 (RB6-8C5, biotin; BD Biosciences), Gr-1 (RB6-8C5, PE; BD Biosciences), Mac-1 (M1/70, biotin; BD Biosciences), Mac-1 (M1/70, PE; BD Biosciences), and Mac-1 (M1/70, APC-Cy7; BD Biosciences). Cells were analyzed by FACS AriaII, FACS SORP Aria, or FACS Canto II (BD Biosciences). Mac-1 was used only in the lineage cocktail for bone marrow. Data were analyzed using FlowJo software (TreeStar).

Transplantation

Sorted cells from *Hlf^{tdTomato/+}* (C57BL/6-Ly5.1/5.2) mice were coinjected intravenously with spleen cells (2×10^5 , Ly5.1) or bone marrow cells (2×10^5 , Ly5.1) into 9.0 Gy (4.5 Gy, each of two doses)-irradiated (C57BL/6-Ly5.2) mice. Secondary transplantation was performed using 5×10^6 or 10^7 bone marrow cells. Repopulation was assayed at 4, 8, 12, and 16 wk after transplantation. Peripheral blood was collected by retro-orbital bleeding under anesthesia. Cells were stained with antibodies to CD45.1 (A20, FITC), CD45.2 (104, APC), Mac-1 (M1/70, PerCP-Cy5.5), Gr-1 (RB6-8C5, PE), B220 (RA3-6B2, PE-Cy7), CD4 (GK1.5, APC-Cy7), and CD8 (53-6.7, APC-Cy7), all purchased from BioLegend. Cells were analyzed by FACS Canto II.

Single-cell microarray analysis

Cells were sorted directly into 4.1 μ l lysis buffer in 96-well plates using the FACS Aria Automated Cell Deposition Unit. Doublets were excluded by forward scatter width/height (FSC-W/FSC-H) and side scatter width/height (SSC-W/SSC-H) gating. To ensure single-cell isolation, we first sorted 220 single cells from an E10.5 embryo into a 96-well plate and examined them under a stereomicroscope. We observed 217 single cells (98.6%) and three vacant wells. Lysis buffer was transferred into a PCR tube, followed by the addition of spike RNA mixture (*Lys*, *Dap*, *Phe*, and *Thr* artificially polyA-tailed RNAs from *Bacillus subtilis* at 1,000, 100, 20, and 5 copies, respectively; American Type Culture Collection; 87482, 87483, 87484, and 87486). Single-cell cDNA amplification was performed as previously described (Kurimoto et al., 2007). Briefly, first-strand cDNAs were synthesized using a poly(dT)-tailed primer. The unreacted primer was eliminated by exonuclease (Takara), and the second strands were generated with a second poly(dT)-tailed primer after poly(dA) addition to the first-strand cDNAs. The quality of cDNAs was assessed by quantitative real-time PCR for house-keeping genes (*Gapdh* and β -actin) and spike RNAs. Template preparation for microarray from the amplified cDNAs was performed as previously described (Kurimoto et al., 2007) with slight modification (T7 promoter addition by 12-cycle PCR, instead of a nine-cycle PCR). Quantity and quality of fragmented

cRNAs were assessed with a RNA 6000 Pico Kit (Agilent Technologies). The qualified cRNA was hybridized to the GeneChip Mouse Genome 430 2.0 Arrays (Affymetrix) according to the manufacturer's instructions. Microarray data processing was performed using the guanine cytosine robust multi-array analysis algorithm implemented in the Bioconductor package *affy*. Because E14.5 HSCs contained less mRNA than E10.5 hematopoietic cluster cells, slight signal saturation was observed in E14.5 HSCs when equal amounts of amplified cRNA were applied to the array chips. This was corrected by the signal intensity of spike RNAs. A heatmap was generated using the *matrix2png* web interface. All microarray data were deposited in Gene Expression Omnibus under accession no. GSE113892.

Quantitative real-time PCR

Real-time PCR was performed using a 7500 Fast Real-Time PCR System (Thermo Fisher Scientific) and Power SYBR Green Master Mix (Applied Biosystems) according to the manufacturer's instructions.

RNA-seq

Random displacement amplification sequencing was performed as previously described (Hayashi et al., 2018). Using 100 sorted cells, first-strand cDNA was synthesized using PrimeScript RT reagent kit (Takara) and not-so-random primers (Ozsolak et al., 2010). Following synthesis of the first strand, the second strand was synthesized using Klenow Fragment (3'-5' exo-; New England Biolabs) and complementary chains of not-so-random primers. After purification of the double-stranded cDNA, the library for RNA-seq was prepared and amplified with a Nextera XT DNA sample Prep Kit (Illumina), according to the manufacturer's instructions. This prepared library was sequenced on a Next-Seq system (Illumina). Each obtained read was mapped to the reference sequence "GRCm38/mm10" using CLC genomic workbench v7.0.4 (Qiagen), and expression levels were normalized and subjected to statistical analyses based on EdgeR. A heatmap was generated using the *matrix2png* web interface. All RNA-seq data were deposited in Gene Expression Omnibus under accession no. GSE114164.

Data analysis

GSEA was performed using GSEA v3.0 (<http://www.broadinstitute.org/gsea/>). Gene sets were obtained from MSigDB (<http://www.broadinstitute.org/gsea/msigdb>), Chambers et al. (2007), Gazit et al. (2013), Mass et al. (2016), Mercher et al. (2008), and Wahlestedt et al. (2017). Gene ontology analysis was performed using the DAVID 6.7 website (<https://david.ncifcrf.gov>).

Western blotting

To make protein extracts for immunoblotting, magnetic-activated cell sorted (Miltenyi Biotec) c-Kit⁺ cells were lysed in radioimmunoprecipitation assay buffer (Cell Signaling). The protein concentration was determined with the BCA protein assay kit (Thermo Fisher Scientific). Equal amounts of protein were denatured, electrophoresed using 12.5% SDS-PAGE, and transferred to a polyvinylidene fluoride membrane. The following primary antibodies were used for immunoblotting

detection: anti-HLF (mouse, 4D8; Santa Cruz Biotechnology), anti-RFP pAb (rabbit; Rockland Immunochemicals), and anti- β -actin (rabbit; Cell Signaling). Goat anti-rabbit IgG (Santa Cruz Biotechnology) and goat anti-mouse IgG (Jackson Immuno-Research) were used as the secondary antibodies. Chemiluminescence was detected using the Pierce ECL Western Blotting Femto kit (Thermo Fisher Scientific), and images were captured using an FX7 camera (Fusion).

Blood cell analysis

Peripheral blood was collected by retro-orbital bleeding under anesthesia, and complete blood cell counts were performed using an automated hematology analyzer, pocH-100i V Diff (Sysmex).

Lymphoid potential assays

For the generation of lymphoid cells, sorted cells were cultured in a T25 culture flask for 11–13 d on an OP9 or OP9-DL1 stromal cell layer in α MEM medium (Gibco) containing 10% FBS and 5×10^{-5} M 2-mercaptoethanol, supplemented with 50 ng/ml of stem cell factor (R&D Systems), 50 ng/ml of FMS-like tyrosine kinase 3 ligand (Flt3L; PeproTech), and 20 ng/ml of IL-7 (R&D Systems). Hematopoietic cells were harvested and analyzed for the expression of surface markers (B cells; B220⁺CD19⁺ cells, T cells; and CD4⁺CD8a⁺ cells) using flow cytometry.

Quantification and statistical analysis

The statistical significance of differences between datasets was determined by Student's *t* test using Prism 6 software (Graph-Pad). All error bars represent SD. Two-tailed *P* values are shown (significance levels: *, *P* < 0.05; **, *P* < 0.01; ***, *P* < 0.001; and ****, *P* < 0.0001).

Online supplemental material

Fig. S1 shows the gating strategy for single-cell microarray analysis. Fig. S2 shows characterization of adult *Hlf*-tdTomato mice. Fig. S3 shows elevation of *Hlf*-tdTomato expression during HSC development. Fig. S4 shows characterization of *Hlf*⁺c-Kit⁺ cells in the yolk sac. Fig. S5 shows RNA-seq analysis of *Hlf*⁺ and *Hlf*⁻ cells.

Acknowledgments

We thank Seiya Mizuno and Marito Araki for designing the targeting construct; Hiroshi Sakamoto, Takashi Moriguchi, and Masayuki Yamamoto for experimental materials; Saori Morino-Koga and Minetaro Ogawa for assistance with lymphoid potential assay; Toshiyuki Kobayashi for Kumamoto earthquake donation; and Takako Ideue for technical assistance.

This work was supported by Japan Society for the Promotion of Science Kakenhi Grant (26461454, 17K09958, and 26221309, Japan) and SENSHIN Medical Research Foundation, the Singapore Ministry of Health's National Medical Research Council under its Singapore Translational Research Investigator Award, and the National Research Foundation Singapore and the Singapore Ministry of Education under its Research Centres of Excellence initiative. We also acknowledge the Research Institute for Diseases of Old Age and the Center for Biomedical Research Resources, Juntendo University School of Medicine.

The authors declare no competing financial interests.

Author contributions: T. Yokomizo conceived the project and designed and performed the research. N. Watanabe made the *Hlf*-tdTomato targeting construct and performed peripheral blood cell analysis. T. Umemoto performed the RNA-seq analysis. J. Matsuo, A. Shimono, and S. Mori assisted with single-cell microarray analysis. Y. Kihara performed Western blotting analysis. R. Harai and H. Takizawa performed whole-mount immunostaining of the bone marrow. E. Nakamura and N. Tada performed ICSI for generating the *Hlf*^{tdTomato/+} mouse. T. Sato and M. Kurokawa contributed analytical tools. N. Nakagata assisted with animal transport and performed in vitro fertilization. T. Yokomizo, T. Takaku, D.G. Tenen, M. Osato, T. Suda, and N. Komatsu participated in project planning. T. Yokomizo, M. Osato, and T. Suda wrote the manuscript.

Submitted: 23 July 2018

Revised: 21 November 2018

Accepted: 19 April 2019

References

- Azcoitia, V. M. Aracil, C. Martínez-A, and M. Torres. 2005. The homeodomain protein Meis1 is essential for definitive hematopoiesis and vascular patterning in the mouse embryo. *Dev. Biol.* 280:307–320. <https://doi.org/10.1016/j.ydbio.2005.01.004>
- Böiers, C. J. Carrelha, M. Lutteropp, S. Luc, J.C. Green, E. Azzoni, P.S. Woll, A.J. Mead, A. Hultquist, G. Swiers, et al. 2013. Lymphomyeloid contribution of an immune-restricted progenitor emerging prior to definitive hematopoietic stem cells. *Cell Stem Cell.* 13:535–548. <https://doi.org/10.1016/j.stem.2013.08.012>
- Boisset, J.C. W. van Cappellen, C. Andrieu-Soler, N. Galjart, E. Dzierzak, and C. Robin. 2010. In vivo imaging of haematopoietic cells emerging from the mouse aortic endothelium. *Nature.* 464:116–120. <https://doi.org/10.1038/nature08764>
- Chambers, S.M. N.C. Boles, K.Y. Lin, M.P. Tierney, T.V. Bowman, S.B. Bradfute, A.J. Chen, A.A. Merchant, O. Sirin, D.C. Weksberg, et al. 2007. Hematopoietic fingerprints: an expression database of stem cells and their progeny. *Cell Stem Cell.* 1:578–591. <https://doi.org/10.1016/j.stem.2007.10.003>
- Chen, M.J. T. Yokomizo, B.M. Zeigler, E. Dzierzak, and N.A. Speck. 2009. Runx1 is required for the endothelial to haematopoietic cell transition but not thereafter. *Nature.* 457:887–891. <https://doi.org/10.1038/nature07619>
- Chen, M.J. Y. Li, M.E. De Obaldia, Q. Yang, A.D. Yzaguirre, T. Yamada-Inagawa, C.S. Vink, A. Bhandoola, E. Dzierzak, and N.A. Speck. 2011. Erythroid/myeloid progenitors and hematopoietic stem cells originate from distinct populations of endothelial cells. *Cell Stem Cell.* 9:541–552. <https://doi.org/10.1016/j.stem.2011.10.003>
- Crisan, M. P. Solaimani Kartalaei, A. Neagu, S. Karkanpouna, T. Yamada-Inagawa, C. Purini, C.S. Vink, R. van der Linden, W. van Ijcken, S.M. Chuva de Sousa Lopes, et al. 2016. BMP and Hedgehog Regulate Distinct AGM Hematopoietic Stem Cells Ex Vivo. *Stem Cell Reports.* 6:383–395. <https://doi.org/10.1016/j.stemcr.2016.01.016>
- de Pater, E. P. Kaimakis, C.S. Vink, T. Yokomizo, T. Yamada-Inagawa, R. van der Linden, P.S. Kartalaei, S.A. Camper, N. Speck, and E. Dzierzak. 2013. Gata2 is required for HSC generation and survival. *J. Exp. Med.* 210:2843–2850. <https://doi.org/10.1084/jem.20130751>
- Dou, D.R. V. Calvanese, M.I. Sierra, A.T. Nguyen, A. Minasian, P. Saarikoski, R. Sasidharan, C.M. Ramirez, J.A. Zack, G.M. Crooks, et al. 2016. Medial HOXA genes demarcate haematopoietic stem cell fate during human development. *Nat. Cell Biol.* 18:595–606. <https://doi.org/10.1038/ncb3354>
- Dzierzak, E. and A. Bigas. 2018. Blood Development: Hematopoietic Stem Cell Dependence and Independence. *Cell Stem Cell.* 22:639–651. <https://doi.org/10.1016/j.stem.2018.04.015>
- Frame, J.M. K.H. Fegan, S.J. Conway, K.E. McGrath, and J. Palis. 2016. Definitive Hematopoiesis in the Yolk Sac Emerges from Wnt-Responsive Hemogenic Endothelium Independently of Circulation and Arterial Identity. *Stem Cells.* 34:431–444. <https://doi.org/10.1002/stem.2213>

- Gazit, R. B.S. Garrison, T.N. Rao, T. Shay, J. Costello, J. Ericson, F. Kim, J.J. Collins, A. Regev, A.J. Wagers, and D.J. Rossi. Immunological Genome Project Consortium. 2013. Transcriptome analysis identifies regulators of hematopoietic stem and progenitor cells. *Stem Cell Reports*. 1:266–280. <https://doi.org/10.1016/j.stemcr.2013.07.004>
- Gekas, C. F. Dieterlen-Lièvre, S.H. Orkin, and H.K. Mikkola. 2005. The placenta is a niche for hematopoietic stem cells. *Dev. Cell*. 8:365–375. <https://doi.org/10.1016/j.devcel.2004.12.016>
- Ghiaur, G. M.J. Ferkowicz, M.D. Milsom, J. Bailey, D. Witte, J.A. Cancelas, M.C. Yoder, and D.A. Williams. 2008. Rac1 is essential for intraembryonic hematopoiesis and for the initial seeding of fetal liver with definitive hematopoietic progenitor cells. *Blood*. 111:3313–3321. <https://doi.org/10.1182/blood-2007-08-110114>
- Gomez Perdiguero, E. K. Klapproth, C. Schulz, K. Busch, E. Azzoni, L. Crozet, H. Garner, C. Trouillet, M.F. de Bruijn, F. Geissmann, and H.R. Rodewald. 2015. Tissue-resident macrophages originate from yolk-sac-derived erythro-myeloid progenitors. *Nature*. 518:547–551. <https://doi.org/10.1038/nature13989>
- Goyama, S. G. Yamamoto, M. Shimabe, T. Sato, M. Ichikawa, S. Ogawa, S. Chiba, and M. Kurokawa. 2008. Evi-1 is a critical regulator for hematopoietic stem cells and transformed leukemic cells. *Cell Stem Cell*. 3: 207–220. <https://doi.org/10.1016/j.stem.2008.06.002>
- Hadland, B.K. S.S. Huppert, J. Kanungo, Y. Xue, R. Jiang, T. Gridley, R.A. Conlon, A.M. Cheng, R. Kopan, and G.D. Longmore. 2004. A requirement for Notch1 distinguishes 2 phases of definitive hematopoiesis during development. *Blood*. 104:3097–3105. <https://doi.org/10.1182/blood-2004-03-1224>
- Hayashi, T. H. Ozaki, Y. Sasagawa, M. Umeda, H. Danno, and I. Nikaido. 2018. Single-cell full-length total RNA sequencing uncovers dynamics of recursive splicing and enhancer RNAs. *Nat. Commun.* 9:619. <https://doi.org/10.1038/s41467-018-02866-0>
- Hoeffel, G. and F. Ginhoux. 2015. Ontogeny of Tissue-Resident Macrophages. *Front. Immunol.* 6:486. <https://doi.org/10.3389/fimmu.2015.00486>
- Hoeffel, G. J. Chen, Y. Lavin, D. Low, F.F. Almeida, P. See, A.E. Beaudin, J. Lum, I. Low, E.C. Forsberg, et al. 2015. C-Myb(+) erythro-myeloid progenitor-derived fetal monocytes give rise to adult tissue-resident macrophages. *Immunity*. 42:665–678. <https://doi.org/10.1016/j.immuni.2015.03.011>
- Inaba, T. W.M. Roberts, L.H. Shapiro, K.W. Jolly, S.C. Raimondi, S.D. Smith, and A.T. Look. 1992. Fusion of the leucine zipper gene HLF to the E2A gene in human acute B-lineage leukemia. *Science*. 257:531–534. <https://doi.org/10.1126/science.1386162>
- Iwasaki, H. F. Arai, Y. Kubota, M. Dahl, and T. Suda. 2010. Endothelial protein C receptor-expressing hematopoietic stem cells reside in the perisinusoidal niche in fetal liver. *Blood*. 116:544–553. <https://doi.org/10.1182/blood-2009-08-240903>
- Kasaai, B. V. Caolo, H.M. Peacock, S. Lehoux, E. Gomez-Perdiguero, A. Luttun, and E.A. Jones. 2017. Erythro-myeloid progenitors can differentiate from endothelial cells and modulate embryonic vascular remodeling. *Sci. Rep.* 7:43817. <https://doi.org/10.1038/srep43817>
- Kataoka, K. T. Sato, A. Yoshimi, S. Goyama, T. Tsuruta, H. Kobayashi, M. Shimabe, S. Arai, M. Nakagawa, Y. Imai, et al. 2011. Evi1 is essential for hematopoietic stem cell self-renewal, and its expression marks hematopoietic cells with long-term multilineage repopulating activity. *J. Exp. Med.* 208:2403–2416. <https://doi.org/10.1084/jem.20110447>
- Kiuseusian, A. P. Brunet de la Grange, O. Burlen-Defranoux, I. Godin, and A. Cumano. 2012. Immature hematopoietic stem cells undergo maturation in the fetal liver. *Development*. 139:3521–3530. <https://doi.org/10.1242/dev.079210>
- Kimura, Y. and R. Yanagimachi. 1995. Intracytoplasmic sperm injection in the mouse. *Biol. Reprod.* 52:709–720. <https://doi.org/10.1095/biolreprod52.4.709>
- Komorowska, K. A. Doyle, M. Wahlestedt, A. Subramaniam, S. Debnath, J. Chen, S. Soneji, B. Van Handel, H.K.A. Mikkola, K. Miharada, et al. 2017. Hepatic Leukemia Factor Maintains Quiescence of Hematopoietic Stem Cells and Protects the Stem Cell Pool during Regeneration. *Cell Reports*. 21:3514–3523. <https://doi.org/10.1016/j.celrep.2017.11.084>
- Kumaravelu, P. L. Hook, A.M. Morrison, J. Ure, S. Zhao, S. Zuyev, J. Ansell, and A. Medvinsky. 2002. Quantitative developmental anatomy of definitive haematopoietic stem cells/long-term repopulating units (HSC/RUs): role of the aorta-gonad-mesonephros (AGM) region and the yolk sac in colonisation of the mouse embryonic liver. *Development*. 129: 4891–4899.
- Kurimoto, K. Y. Yabuta, Y. Ohinata, and M. Saitou. 2007. Global single-cell cDNA amplification to provide a template for representative high-density oligonucleotide microarray analysis. *Nat. Protoc.* 2:739–752. <https://doi.org/10.1038/nprot.2007.79>
- Lee, L.K. Y. Ghorbanian, W. Wang, Y. Wang, Y.J. Kim, I.L. Weissman, M.A. Inlay, and H.K.A. Mikkola. 2016. LYVE1 Marks the Divergence of Yolk Sac Definitive Hemogenic Endothelium from the Primitive Erythroid Lineage. *Cell Reports*. 17:2286–2298. <https://doi.org/10.1016/j.celrep.2016.10.080>
- Li, Y. L. Gao, B. Hadland, K. Tan, and N.A. Speck. 2017. CD27 marks murine embryonic hematopoietic stem cells and type II prehematopoietic stem cells. *Blood*. 130:372–376. <https://doi.org/10.1182/blood-2017-03-776849>
- Li, Z. Y. Lan, W. He, D. Chen, J. Wang, F. Zhou, Y. Wang, H. Sun, X. Chen, C. Xu, et al. 2012. Mouse embryonic head as a site for hematopoietic stem cell development. *Cell Stem Cell*. 11:663–675. <https://doi.org/10.1016/j.stem.2012.07.004>
- Lux, C.T. M. Yoshimoto, K. McGrath, S.J. Conway, J. Palis, and M.C. Yoder. 2008. All primitive and definitive hematopoietic progenitor cells emerging before E10 in the mouse embryo are products of the yolk sac. *Blood*. 111:3435–3438. <https://doi.org/10.1182/blood-2007-08-107086>
- Mass, E. I. Ballesteros, M. Farlik, F. Halbritter, P. Günther, L. Crozet, C.E. Jacome-Galarza, K. Händler, J. Klughammer, Y. Kobayashi, et al. 2016. Specification of tissue-resident macrophages during organogenesis. *Science*. 353:aaf4238. <https://doi.org/10.1126/science.aaf4238>
- McGrath, K.E. J.M. Frame, and J. Palis. 2015b. Early hematopoiesis and macrophage development. *Semin. Immunol.* 27:379–387. <https://doi.org/10.1016/j.smim.2016.03.013>
- McGrath, K.E. J.M. Frame, K.H. Fegan, J.R. Bowen, S.J. Conway, S.C. Catherman, P.D. Kingsley, A.D. Koniski, and J. Palis. 2015a. Distinct Sources of Hematopoietic Progenitors Emerge before HSCs and Provide Functional Blood Cells in the Mammalian Embryo. *Cell Reports*. 11:1892–1904. <https://doi.org/10.1016/j.celrep.2015.05.036>
- Medvinsky, A. S. Rybtsov, and S. Taoudi. 2011. Embryonic origin of the adult hematopoietic system: advances and questions. *Development*. 138: 1017–1031. <https://doi.org/10.1242/dev.040998>
- Mercher, T. M.G. Cornejo, C. Sears, T. Kindler, S.A. Moore, I. Maillard, W.S. Pear, J.C. Aster, and D.G. Gilliland. 2008. Notch signaling specifies megakaryocyte development from hematopoietic stem cells. *Cell Stem Cell*. 3:314–326. <https://doi.org/10.1016/j.stem.2008.07.010>
- Mucenski, M.L. K. McLain, A.B. Kier, S.H. Swerdlow, C.M. Schreiner, T.A. Miller, D.W. Pietryga, W.J. Scott Jr. and S.S. Potter. 1991. A functional c-myb gene is required for normal murine fetal hepatic hematopoiesis. *Cell*. 65:677–689. [https://doi.org/10.1016/0092-8674\(91\)90099-K](https://doi.org/10.1016/0092-8674(91)90099-K)
- Ng, C.E. T. Yokomizo, N. Yamashita, B. Cirovic, H. Jin, Z. Wen, Y. Ito, and M. Osato. 2010. A Runx1 intronic enhancer marks hemogenic endothelial cells and hematopoietic stem cells. *Stem Cells*. 28:1869–1881. <https://doi.org/10.1002/stem.507>
- Ng, E.S. L. Azzola, F.F. Bruveris, V. Calvanese, B. Phipson, K. Vlahos, C. Hirst, V.J. Jokubaitis, Q.C. Yu, J. Maksimovic, et al. 2016. Differentiation of human embryonic stem cells to HOXA⁺ hemogenic vasculature that resembles the aorta-gonad-mesonephros. *Nat. Biotechnol.* 34:1168–1179. <https://doi.org/10.1038/nbt.3702>
- Orkin, S.H. and L.I. Zon. 2008. Hematopoiesis: an evolving paradigm for stem cell biology. *Cell*. 132:631–644. <https://doi.org/10.1016/j.cell.2008.01.025>
- Ozsolak, F. A. Goren, M. Gymrek, M. Guttman, A. Regev, B.E. Bernstein, and P.M. Milos. 2010. Digital transcriptome profiling from attomole-level RNA samples. *Genome Res.* 20:519–525. <https://doi.org/10.1101/gr.102129.109>
- Padrón-Barthe, L. S. Temiño, C. Villa del Campo, L. Carramolino, J. Isern, and M. Torres. 2014. Clonal analysis identifies hemogenic endothelium as the source of the blood-endothelial common lineage in the mouse embryo. *Blood*. 124:2523–2532. <https://doi.org/10.1182/blood-2013-12-545939>
- Perdiguero, E.G. and F. Geissmann. 2016. The development and maintenance of resident macrophages. *Nat. Immunol.* 17:2–8. <https://doi.org/10.1038/ni.3341>
- Perdiguero, E.G. K. Klapproth, C. Schulz, K. Busch, M. de Bruijn, H.R. Rodewald, and F. Geissmann. 2015. The Origin of Tissue-Resident Macrophages: When an Erythro-myeloid Progenitor Is an Erythro-myeloid Progenitor. *Immunity*. 43:1023–1024. <https://doi.org/10.1016/j.immuni.2015.11.022>
- Rhodes, K.E. C. Gekas, Y. Wang, C.T. Lux, C.S. Francis, D.N. Chan, S. Conway, S.H. Orkin, M.C. Yoder, and H.K. Mikkola. 2008. The emergence of hematopoietic stem cells is initiated in the placental vasculature in the absence of circulation. *Cell Stem Cell*. 2:252–263. <https://doi.org/10.1016/j.stem.2008.01.001>
- Riddell, J. R. Gazit, B.S. Garrison, G. Guo, A. Saadatpour, P.K. Mandal, W. Ebina, P. Volchkov, G.C. Yuan, S.H. Orkin, and D.J. Rossi. 2014.

- Reprogramming committed murine blood cells to induced hematopoietic stem cells with defined factors. *Cell*. 157:549–564. <https://doi.org/10.1016/j.cell.2014.04.006>
- Rowe, R.G. J. Mandelbaum, L.I. Zon, and G.Q. Daley. 2016. Engineering Hematopoietic Stem Cells: Lessons from Development. *Cell Stem Cell*. 18: 707–720. <https://doi.org/10.1016/j.stem.2016.05.016>
- Rybtsov, S. A. Ivanovs, S. Zhao, and A. Medvinsky. 2016. Concealed expansion of immature precursors underpins acute burst of adult HSC activity in foetal liver. *Development*. 143:1284–1289. <https://doi.org/10.1242/dev.131193>
- Sakamoto, H. N. Takeda, F. Arai, K. Hosokawa, P. Garcia, T. Suda, J. Frampton, and M. Ogawa. 2015. Determining c-Myb protein levels can isolate functional hematopoietic stem cell subtypes. *Stem Cells*. 33: 479–490. <https://doi.org/10.1002/stem.1855>
- Samokhvalov, I.M. N.I. Samokhvalova, and S. Nishikawa. 2007. Cell tracing shows the contribution of the yolk sac to adult haematopoiesis. *Nature*. 446:1056–1061. <https://doi.org/10.1038/nature05725>
- Schulz, C. E. Gomez Perdiguero, L. Chorro, H. Szabo-Rogers, N. Cagnard, K. Kierdorf, M. Prinz, B. Wu, S.E. Jacobsen, J.W. Pollard, et al. 2012. A lineage of myeloid cells independent of Myb and hematopoietic stem cells. *Science*. 336:86–90. <https://doi.org/10.1126/science.1219179>
- Shojaei, F. J. Trowbridge, L. Gallacher, L. Yuefei, D. Goodale, F. Karanu, K. Levac, and M. Bhatia. 2005. Hierarchical and ontogenic positions serve to define the molecular basis of human hematopoietic stem cell behavior. *Dev. Cell*. 8:651–663. <https://doi.org/10.1016/j.devcel.2005.03.004>
- Sturgeon, C.M. A. Ditadi, G. Awong, M. Kennedy, and G. Keller. 2014. Wnt signaling controls the specification of definitive and primitive hematopoiesis from human pluripotent stem cells. *Nat. Biotechnol.* 32: 554–561. <https://doi.org/10.1038/nbt.2915>
- Swiers, G. C. Baumann, J. O'Rourke, E. Giannoulata, S. Taylor, A. Joshi, V. Moignard, C. Pina, T. Bee, K.D. Kokkalis, et al. 2013. Early dynamic fate changes in haemogenic endothelium characterized at the single-cell level. *Nat. Commun.* 4:2924. <https://doi.org/10.1038/ncomms3924>
- Taoudi, S. C. Gonneau, K. Moore, J.M. Sheridan, C.C. Blackburn, E. Taylor, and A. Medvinsky. 2008. Extensive hematopoietic stem cell generation in the AGM region via maturation of VE-cadherin+CD45+ pre-definitive HSCs. *Cell Stem Cell*. 3:99–108. <https://doi.org/10.1016/j.stem.2008.06.004>
- Tober, J. M.M.W. Maijenburg, Y. Li, L. Gao, B.K. Hadland, P. Gao, K. Minoura, I.D. Bernstein, K. Tan, and N.A. Speck. 2018. Maturation of hematopoietic stem cells from prehematopoietic stem cells is accompanied by up-regulation of PD-L1. *J. Exp. Med.* 215:645–659. <https://doi.org/10.1084/jem.20161594>
- Vo, L.T. M.A. Kinney, X. Liu, Y. Zhang, J. Barragan, P.M. Sousa, D.K. Jha, A. Han, M. Cesana, Z. Shao, et al. 2018. Regulation of embryonic haematopoietic multipotency by EZH1. *Nature*. 553:506–510. <https://doi.org/10.1038/nature25435>
- Wahlestedt, M. V. Ladopoulos, I. Hidalgo, M. Sanchez Castillo, R. Hannah, P. Säwén, H. Wan, M. Dudenhöffer-Pfeifer, M. Magnusson, G.L. Norddahl, et al. 2017. Critical Modulation of Hematopoietic Lineage Fate by Hepatic Leukemia Factor. *Cell Reports*. 21:2251–2263. <https://doi.org/10.1016/j.celrep.2017.10.112>
- Yokomizo, T. and E. Dzierzak. 2010. Three-dimensional cartography of hematopoietic clusters in the vasculature of whole mouse embryos. *Development*. 137:3651–3661. <https://doi.org/10.1242/dev.051094>
- Yokomizo, T. T. Yamada-Inagawa, A.D. Yzaguirre, M.J. Chen, N.A. Speck, and E. Dzierzak. 2012. Whole-mount three-dimensional imaging of internally localized immunostained cells within mouse embryos. *Nat. Protoc.* 7:421–431. <https://doi.org/10.1038/nprot.2011.441>
- Yzaguirre, A.D. and N.A. Speck. 2016. Insights into blood cell formation from hemogenic endothelium in lesser-known anatomic sites. *Dev. Dyn.* 245: 1011–1028. <https://doi.org/10.1002/dvdy.24430>
- Zhen, F. Y. Lan, B. Yan, W. Zhang, and Z. Wen. 2013. Hemogenic endothelium specification and hematopoietic stem cell maintenance employ distinct Scl isoforms. *Development*. 140:3977–3985. <https://doi.org/10.1242/dev.097071>
- Zhou, F. X. Li, W. Wang, P. Zhu, J. Zhou, W. He, M. Ding, F. Xiong, X. Zheng, Z. Li, et al. 2016. Tracing haematopoietic stem cell formation at single-cell resolution. *Nature*. 533:487–492. <https://doi.org/10.1038/nature17997>
- Zovein, A.C. J.J. Hofmann, M. Lynch, W.J. French, K.A. Turlo, Y. Yang, M.S. Becker, L. Zanetta, E. Dejana, J.C. Gasson, et al. 2008. Fate tracing reveals the endothelial origin of hematopoietic stem cells. *Cell Stem Cell*. 3: 625–636. <https://doi.org/10.1016/j.stem.2008.09.018>